Thermochronology and tectonics of the Leeward Antilles: Evolution of the southern Caribbean Plate boundary zone

Roelant van der Lelij,[1] Richard A. Spikings,[1] Andrew C. Kerr,[2] Alexandre Kounov,[3] Michael Cosca,[4] David Chew,[5] and Diego Villagomez[1]

Received 19 December 2009; revised 13 April 2010; accepted 7 June 2010; published 11 November 2010.

[1] Tectonic reconstructions of the Caribbean Plate are severely hampered by a paucity of geochronologic and exhumation constraints from anastomosed basement blocks along its southern margin. New U/Pb, $^{40}Ar/^{39}Ar$, apatite fission track, and apatite (U-Th)/He data constrain quantitative thermal and exhumation histories, which have been used to propose a model for the tectonic evolution of the emergent parts of the Bonaire Block and the southern Caribbean Plate boundary zone. An east facing arc system intruded through an oceanic plateau during ~90 to ~87 Ma and crops out on Aruba. Subsequent structural displacements resulted in >80°C of cooling on Aruba during 70–60 Ma. In contrast, exhumation of the island arc sequence exposed on Bonaire occurred at 85–80 Ma and 55–45 Ma. Santonian exhumation on Bonaire occurred immediately subsequent to burial metamorphism and may have been driven by the collision of a west facing island arc with the Caribbean Plate. Island arc rocks intruded oceanic plateau rocks on Gran Roque at ~65 Ma and exhumed rapidly at 55–45 Ma. We attribute Maastrichtian-Danian exhumation on Aruba and early Eocene exhumation on Bonaire and Gran Roque to sequential diachronous accretion of their basement units to the South American Plate. Widespread unconformities indicate late Eocene subaerial exposure. Late Oligocene–early Miocene dextral transtension within the Bonaire Block drove subsidence and burial of crystalline basement rocks of the Leeward Antilles to ≤1 km. Late Miocene–recent transpression caused inversion and ≤1 km of exhumation, possibly as a result of the northward escape of the Maracaibo Block. **Citation:** van der Lelij, R., R. A. Spikings, A. C. Kerr, A. Kounov, M. Cosca, D. Chew, and D. Villagomez (2010), Thermochronology and tectonics of the Leeward Antilles: Evolution of the southern Caribbean Plate boundary zone, *Tectonics*, *29*, TC6003, doi:10.1029/2009TC002654.

[1]Department of Mineralogy, University of Geneva, Geneva, Switzerland.
[2]School of Earth and Ocean Sciences, Cardiff University, Cardiff, UK.
[3]Institute of Geology and Paleontology, University of Basel, Basel, Switzerland.
[4]U.S. Geological Survey, Denver, Colorado, USA.
[5]Department of Geology, School of Natural Sciences, Trinity College, Dublin, Ireland.

0278-7407/10/2009TC002654

1. Introduction

[2] Any kinematic reconstruction of the Caribbean Plate must take into account the tectonic evolution of the spatially diffuse, Late Cretaceous–recent South Caribbean Plate boundary zone (SCPBZ; Figure 1). This fault zone hosts numerous anastomosed blocks, whose tectonic histories are linked to the displacement of the Caribbean Plate relative to South America. Contrasting lithologies between the basements of these blocks suggests that they formed in different geological settings. Furthermore, significant variations in sedimentary successions and topography suggest they have highly varied exhumation and burial histories. We aim to quantify the burial and exhumation histories of the entrained Bonaire Block to constrain the tectonic history of the SCPBZ and provide temporal limits on the kinematic evolution of the Caribbean Plate.

[3] The Bonaire Block hosts the Leeward Antilles (Figure 2), which have sparse pre-Miocene sedimentary cover, exposing a large area of crystalline basement that is amenable to analysis using a variety of geochronological and thermochronological methods. Nevertheless, previous tectonic reconstructions of the Bonaire Block have been hampered by a paucity of accurate, quantitative data, rendering any temporal control on the evolution of the southern Caribbean Plate to be tentative. Consequently, previous interpretations of the evolution of the Bonaire Block are highly varied [e.g., *Beets et al.*, 1984; *Priem*, 1979; *Priem et al.*, 1966; *Santamaría and Schubert*, 1974; *White et al.*, 1999].

[4] This study attempts to reconstruct the tectonic evolution of the Bonaire Block, by combining new U/Pb, $^{40}Ar/^{39}Ar$, apatite fission track and apatite (U-Th)/He data with existing radiometric data to generate thermal histories of crystalline rocks. These histories have been combined with the sedimentary record to define exhumation histories, assuming a constant, linear geothermal gradient since 90 Ma. This paper constrains the timing of collision of the Caribbean Plate with South America, and provides bounds for the evolution of subduction dynamics and arc evolution at collision zones between ocean plateaus and MORB, intraoceanic arcs and continental crust, such as along the margins of the Caribbean and the Ontong-Java plateaus.

2. Geological Framework and Previous Work

[5] A majority of models for the allochthonous evolution of the Caribbean region shows that the Caribbean Plate originated in the Pacific realm, and was entrapped in the space between the North and South American Plates as these migrated westward [e.g., *Pindell et al.*, 2005]. Subsequent

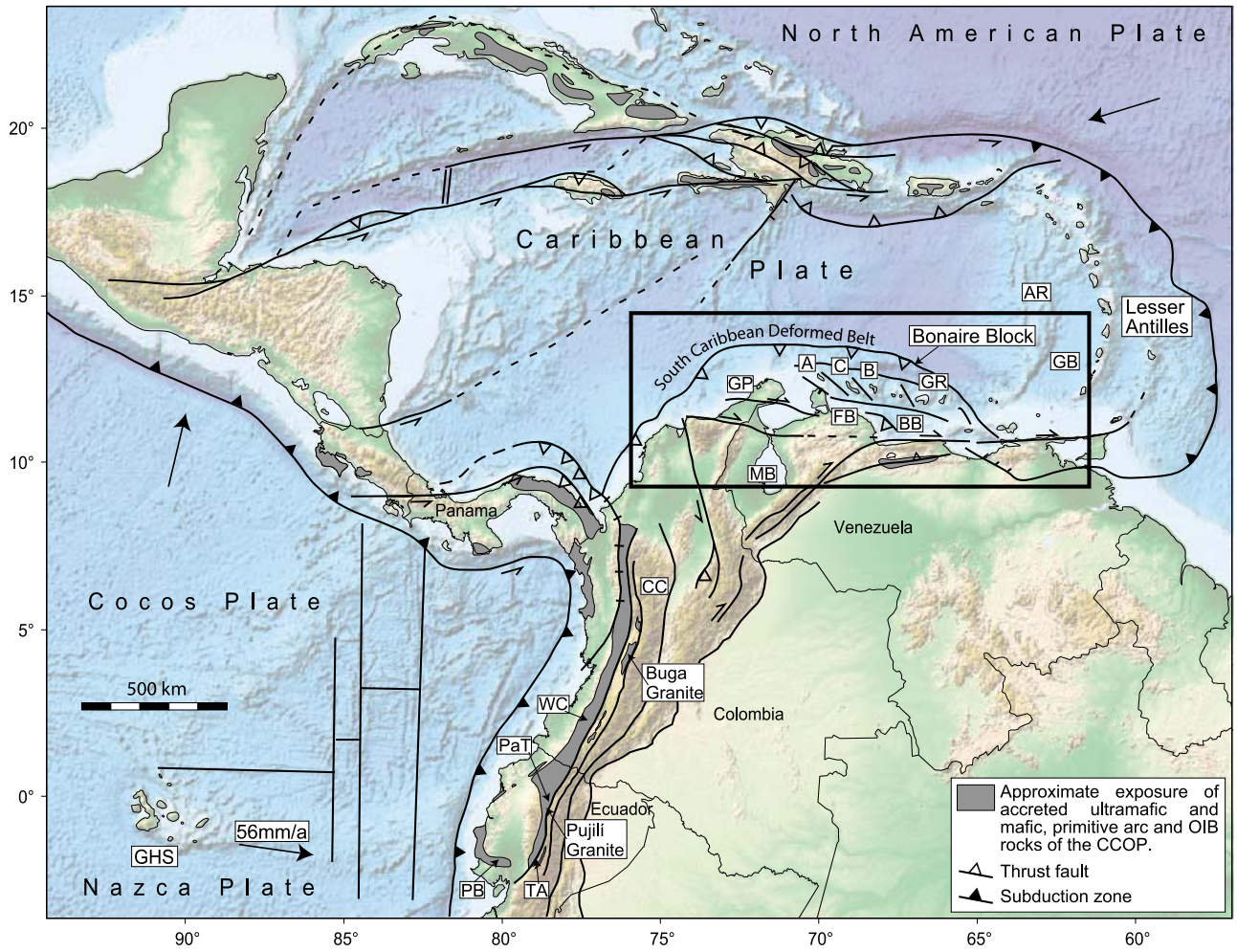

Figure 1. Digital elevation model of the northern South American and Caribbean plates (ETOPO1 [*Amante and Eakins*, 2008]). Accreted fragments of the Caribbean Cretaceous Oceanic Province are shown (modified from *Kerr et al.* [2003]), and the southern Caribbean Plate boundary zone is highlighted by the black rectangle. Plate vectors are from *Norabuena et al.* [1999] and *DeMets et al.* [2000]. A, Aruba; AR, Aves Ridge; B, Bonaire; BB, Bonaire Basin; C, Curacao; CC, Central Cordillera of Colombia; FB, Falcón Basin; GB, Grenada Basin; GHS, Galapagos Hot Spot; GP, Guajira Peninsula; GR, Gran Roque; MB, Maracaibo Block; PB, Piñon Block; PaT, Pallatanga Block; TA, Totoras Amphibolite (Ecuador); WC, Western Cordillera of Colombia.

displacement between the Caribbean, South American and North American plates generated broad strike-slip zones, with juxtaposed transtensive and transpressive regions along the northern and southern boundaries of the Caribbean Plate [*Pindell et al.*, 2005]. The SCPBZ hosts distinct structural, crystalline blocks that are either allochthonous fragments of oceanic crust (e.g., the Bonaire Block), or para-autochthonous fragments of the continental South American Plate (e.g., the Maracaibo Block; Figure 1).

2.1. Caribbean Plate

[6] The submerged portion of the Caribbean Plate is mainly composed of an 8–20 km thick [*Edgar et al.*, 1971] ultramafic and mafic basement with an oceanic plateau geochemical and isotopic affinity [*Sinton et al.*, 1998], which has accreted and crops out in scattered locations throughout the Caribbean region and along northwestern and northern South America (Figure 1). The thickened crust erupted in two plate-wide pulses at ~91–88 Ma and ~76 Ma [*Sinton et al.*, 1998] and is commonly referred to as the Caribbean Colombian Oceanic Plateau (CCOP). Commonly cited models for voluminous outpourings of the oceanic plateau include eruption of melt above a mantle plume, for example near the Galapagos hot spot [e.g., *Kerr et al.*, 1996].

[7] Some authors argue for an almost autochthonous inter-American origin for the Caribbean Plate [*Meschede and Frisch*, 1998; *James*, 2006] implying very little movement relative to the North and South American plates. In contrast, a significant amount of evidence supports a Pacific origin, such as (1) the distribution of ~90 Ma old oceanic plateau

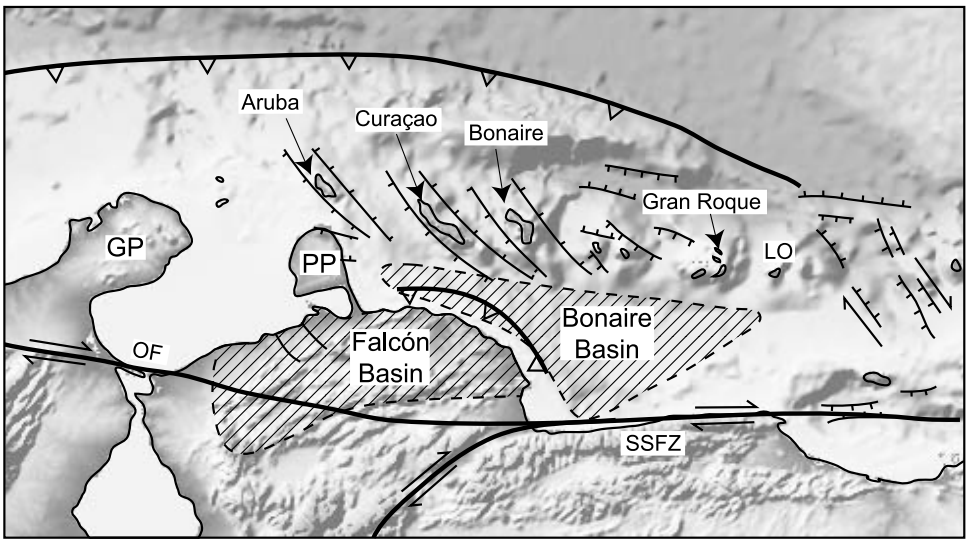

Figure 2. Digital elevation model of the Leeward Antilles (ETOPO1 [*Amante and Eakins*, 2008]). Shaded areas defined by dashed lines mark the geographical extensions of the Bonaire and Falcón basins [*Gorney et al.*, 2007]. Structure is compiled from *Curet* [1992] and *Gorney et al.* [2007]. GP, Guajira Peninsula; LO, La Orchila; OF, Oca Fault; SSFZ, San Sebastian Fault Zone.

rocks along the northwestern margin of the South American Plate [*Kerr et al.*, 1996; *Spikings et al.*, 2005; *Luzieux et al.*, 2006; *Vallejo et al.*, 2006] (Figure 1) and (2) the presence of Pacific fauna within the Caribbean region [*Montgomery et al.*, 1994; *Baumgartner et al.*, 2004], leading to models such as those proposed by *Pindell and Dewey* [1982], *Burke* [1988], *Ross and Scotese* [1988] and *Pindell et al.* [2005].

[8] Thermochronological and sedimentological analyses of accreted oceanic crust and the paleocontinental margin in Ecuador and Colombia shows that the CCOP collided with the South American Plate at ~75–73 Ma [*Spikings et al.*, 2000; *Villagómez et al.*, 2008; *Vallejo et al.*, 2009] as it drifted northeastward. Subsequent migration of the fragmented Caribbean Plate into the intra-American gap consumed the Jurassic spreading center of the proto-Caribbean seaway by subduction beneath the leading edge of the Caribbean Plate, resulting in the onset of convergence between the North and South American plates in the Eocene [*Pindell et al.*, 2005]. Contemporaneously, consumption of proto-Caribbean crust on the northern plate boundary resulted in the collision of the Cuban arc terranes with the Bahama Banks. Consequently, northern plate boundary conditions changed from convergent to sinistral strike slip, which led to a change of plate motion direction, due eastward [*Pindell et al.*, 2005]. Oblique underthrusting of Caribbean oceanic crust was amagmatic along the southern plate boundary [*Audemard and Audemard*, 2002], and formed the South Caribbean Deformed Belt in the Paleogene [*Pindell and Barrett*, 1990; *Gorney et al.*, 2007] or in the Miocene-Pliocene [*Audemard and Audemard*, 2002].

[9] From the Eocene onward, the SCPBZ went from obliquely convergent to a complex, dominantly strike-slip transpressive margin with local transtension [e.g., *Audemard et al.*, 2005]. High-resolution seismic data [*Gorney et al.*, 2007] reveal extension in the Leeward Antilles basement during the late Eocene, opening the Bonaire and Falcón basins (Figure 2), and in the late Oligocene–early Miocene, creating rift basins between the Leeward Antilles islands. Transpression starting in the middle Miocene drove inversion of previous normal faults [*Gorney et al.*, 2007]. Suturing of the Panama–Costa Rica arc, which started at ~10 Ma [*Kellogg*, 1984; *Mann and Burke*, 1984] or at ~5 Ma [*Audemard*, 1998], resulted in E-W oriented compression, which extruded the Maracaibo and Bonaire blocks (Figure 1) to the NNE by ~290 km with respect to stable cratonic South America [*Dewey and Pindell*, 1985]. This resulted in the late Miocene Andean orogeny in Venezuela [*Kohn et al.*, 1984], deformation in the South Caribbean Deformed Belt and the dramatic topography of the Sierra Nevada de Santa Marta [*Silver et al.*, 1975]. The horizontal distance of underthrusting of the Caribbean slab beneath the Bonaire Block is estimated between 150 and 250 km, based on geophysical data [*Bezada et al.*, 2008; *van der Hilst and Mann*, 1994].

2.2. Geological Framework of the Leeward Antilles

[10] The Leeward Antilles islands appear to have very distinct geological histories, and it has been proposed that their juxtaposition in the Bonaire Block occurred after they were transported and extracted from their original tectonic setting by accretion to the South American margin [*Thompson et al.*, 2004].

2.2.1. Aruba

[11] Aruba consists of a Late Cretaceous, heterogeneous tonalitic batholith, which intrudes the basaltic-doleritic Aruba Lava Formation (Figure 3). The Turonian age (93.6 ± 0.8 – ~88.6 Ma [*Gradstein et al.*, 2004]) of the Aruba Lava Formation is constrained by ammonites within intercalated

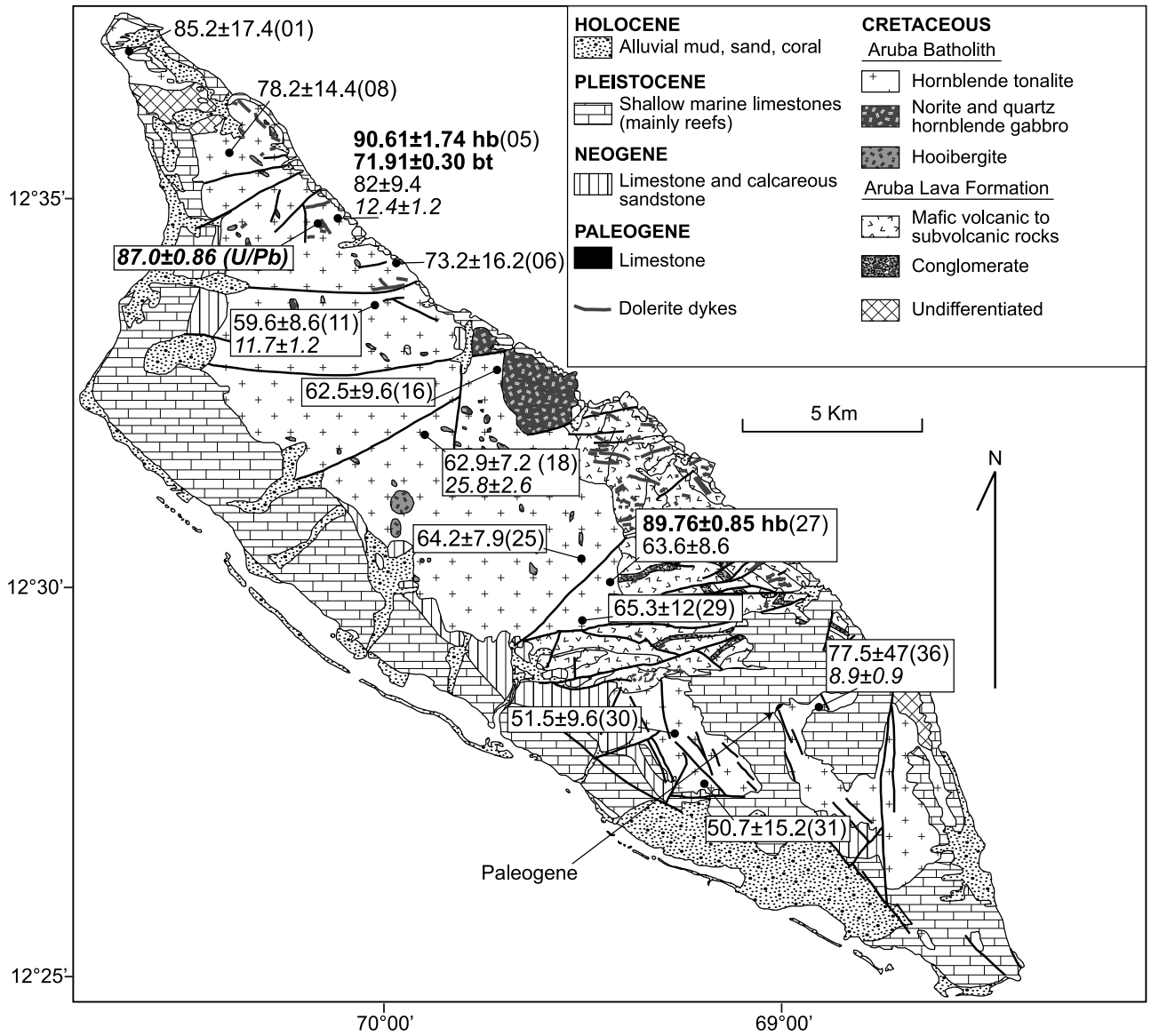

Figure 3. Geological map of Aruba after *Beets et al.* [1996] showing the exposure of the Aruba Lava Formation and the Aruba Batholith. Sample locations and ages are shown, and labels are U/Pb ages (Ma ± 2σ in bold italic text), $^{40}Ar/^{39}Ar$ ages (Ma ± 2σ in bold text: hb, hornblende; bt, biotite total fusion), apatite fission track ages (Ma ± 2σ in normal text), and apatite (U-Th)/He ages (Ma ± 2σ in italic text), with sample codes shown in parentheses (06VDLxx).

sedimentary strata [*MacDonald*, 1968; *Beets et al.*, 1984]. Radiometric dating of the Aruba Lava Formation has been hindered by pervasive alteration [*White et al.*, 1999], although the fossil age overlaps with radiometric ages obtained from the neighboring Curaçao Lava Formation (88.9 ± 0.8 Ma [*Sinton et al.*, 1998]), suggesting a common origin. In addition, both lava formations yield geochemical and isotopic E-MORB to T-MORB signatures [*White et al.*, 1999], leading *White et al.* [1999] to conclude that the Aruba Lava Formation is an obducted part of the CCOP. Field studies show that the Aruba Lava Formation was buried, sheared and regionally metamorphosed prior to batholith intrusion [e.g., *Wright and Wyld*, 2004].

[12] The Aruba Batholith intrudes and contact metamorphoses the mafic plateau sequences up to amphibolite-hornfels facies [*Helmers and Beets*, 1977; *White et al.*, 1999]. A majority of previous attempts to radiometrically date the Aruba Batholith utilized the Rb/Sr and K/Ar methods, and yielded widely varying ages (>90 Ma–60 Ma; Figure 4). This discordance is a result of partial daughter isotope loss, indicating either that (1) the batholith underwent slow cooling after emplacement, (2) they were thermally disturbed by later magmatic activity or by burial, or (3) the rocks were altered. More recently, zircon U/Pb [*Wright and Wyld*, 2004] (see also this study) ages spanning between 89 ± 1 and 87.0 ± 0.9 Ma record the crystallization

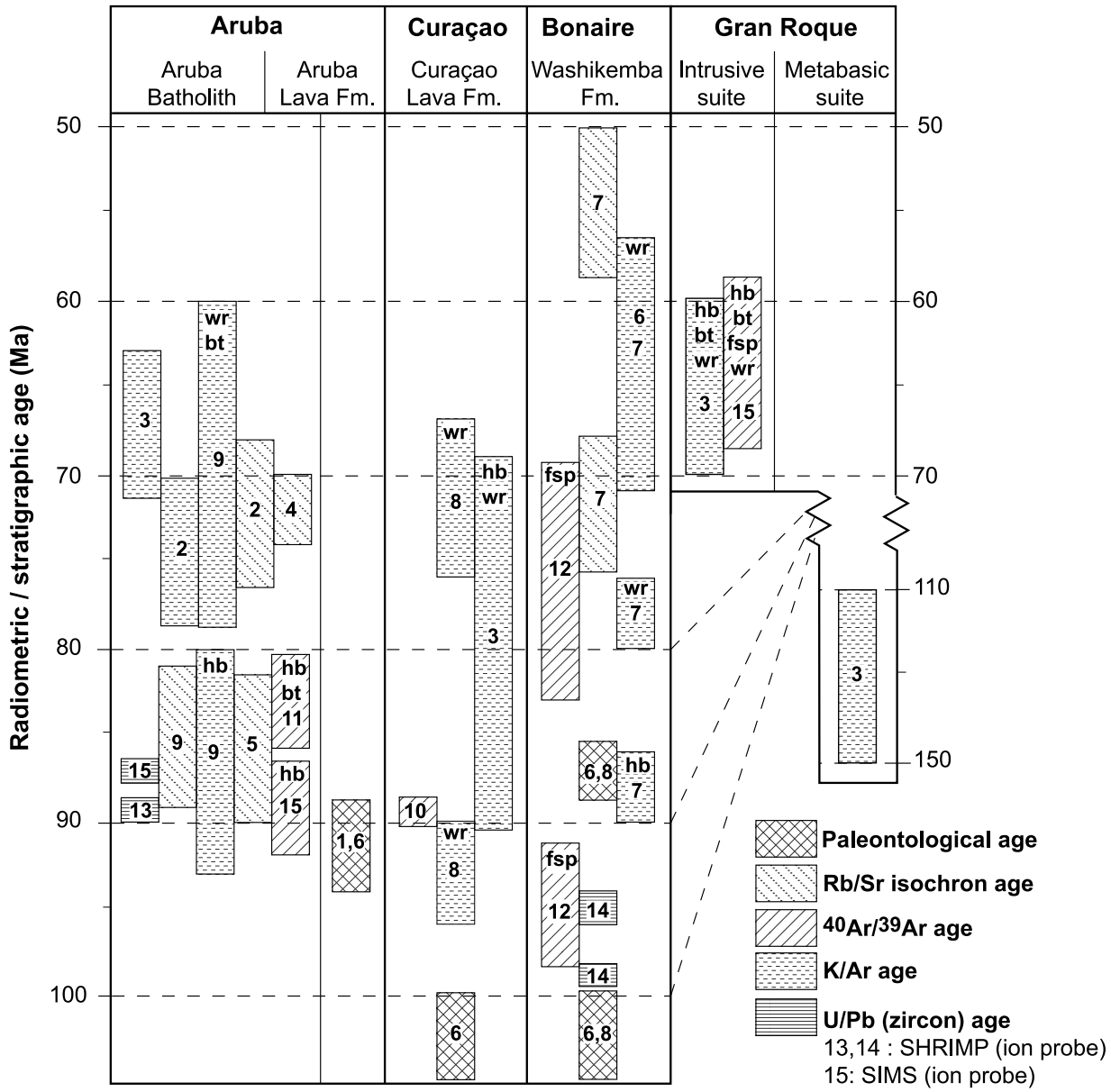

Figure 4. Summary of radiometric and fossil age data from the igneous basement sequences of the Leeward Antilles. Only radiometric systems with closure temperatures >150°C are shown. Bt, biotite; hb, hornblende; fsp, feldspar; wr, whole rock. Here 1, *MacDonald* [1968]; 2, *Priem et al.* [1966]; 3, *Santamaría and Schubert* [1974]; 4, *Priem et al.* [1977]; 5, *Priem et al.* [1978]; 6, *Wiedmann* [1978]; 7, *Priem et al.* [1978]; 8, *Beets et al.* [1984]; 9, *Priem et al.* [1986a]; 10, *Sinton et al.* [1998]; 11, *White et al.* [1999]; 12, *Thompson et al.* [2004]; 13, *Wright and Wyld* [2004]; 14, J. E. Wright (personal communication, 2008); 15, this study (concordant or plateau ages only).

age of the batholith. *White et al.* [1999] present hornblende $^{40}Ar/^{39}Ar$ ages that range between ~87 to ~82 Ma, although they did not present any Ar age spectra or isotopic data, rendering their ages uninterpretable. Negative Nb and Ti anomalies led *White et al.* [1999] and *Thompson et al.* [2004] to suggest that the Aruba Batholith originated either by west dipping subduction beneath the plateau, or by partial anatexis of hydrated amphibole bearing plateau rocks in the absence of a subduction zone, yielding their tonalite-trondhjemite-granodiorite (TTG) geochemical affinity [see also *Condie*, 2005; *Willbold et al.*, 2009]. *Beardsley* [2007] performed apatite fission track analyses in combination with a fluid inclusion study to constrain the thermal history of the Aruba Batholith. The combined effects of low uranium contents and abundant dislocations in the apatite grains precluded the acquisition of precise ages and track lengths, and therefore the two AFT ages of 87 ± 33 and 69 ± 20 Ma only loosely constrain the cooling history of Aruba.

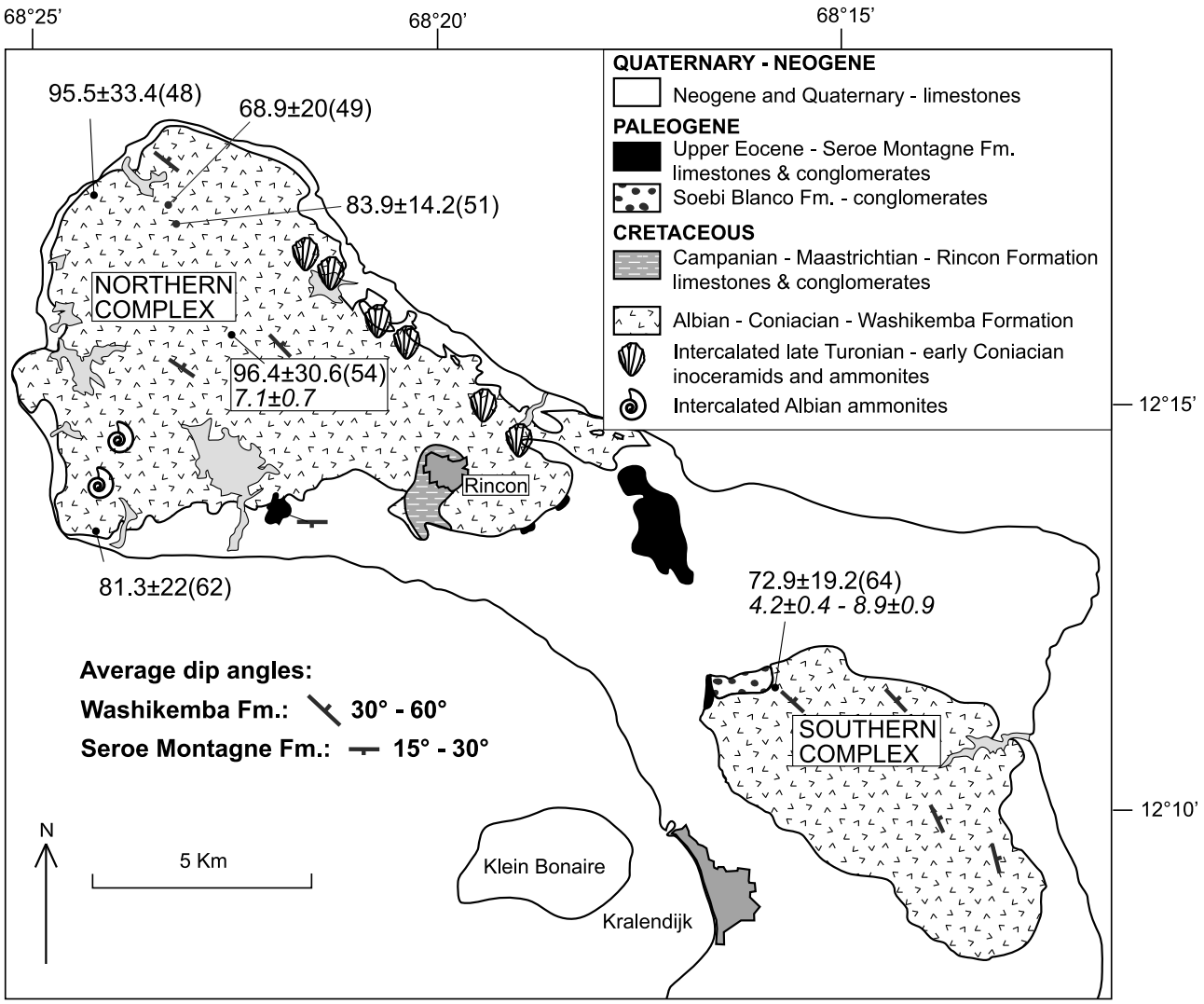

Figure 5. Geological map of Bonaire simplified after *Pijpers* [1933] and *Beets et al.* [1977] showing the exposure of the Washikemba Formation within the northern and southern complexes. Sample locations are shown, and labels are apatite fission track ages (Ma ± 2σ in normal text) and apatite (U-Th)/He ages (Ma ± 2σ in italic text), with sample codes shown in parentheses (06VDLxx).

[13] The oldest overlying sedimentary rocks are Eocene or Oligocene, and are exposed in small erosional outliers in the southeastern part of the island [*Beets et al.*, 1996]. Early Miocene mudstones and sandstones were intercepted in a borehole in the center of Oranjestad [*Helmers and Beets*, 1977]. Dolomitic limestones of the late Miocene–Pliocene Seroe Domi Formation are widespread along the southeastern part of the island [*Beets et al.*, 1996].

2.2.2. Bonaire

[14] The basement of Bonaire is represented by the >5 km thick Washikemba Formation, which mainly consists of submarine volcaniclastic rocks and associated rhyodacitic and dacitic sills and flows [*Klaver*, 1976]. The formation crops out in two inliers located in northern (Northern Complex) and central (Southern Complex; Figure 5) Bonaire, and neither the base nor the top of the formation are exposed [*Beets et al.*, 1977]. The Washikemba Formation was metamorphosed to at least prehnite-pumpellyite facies [*Thompson et al.*, 2004], and tilted by 30° to 60° to the northeast prior to deposition of the overlying Cretaceous sedimentary rocks [*Pijpers*, 1933].

[15] Previous $^{40}Ar/^{39}Ar$, K/Ar and Rb/Sr data obtained from the dacites to rhyolites range between 100 Ma and 57.0 Ma (Figure 4), and were accounted for by the competing effects of daughter isotope loss and excess ^{40}Ar [*Priem*, 1979; *Thompson et al.*, 2004]. *Beets et al.* [1977] report Albian (112 ± 1 to 99.6 ± 1 Ma) ammonites in sedimentary strata at the base of the Northern Complex, and *Kauffman* [1978] reports late Turonian–early Coniacian (88.6–85.8 ± 0.7 Ma) inoceramids and early Coniacian ammonites in a sedimentary layer at the top of the Northern Complex. Unpublished U/Pb RG-SHRIMP (zircon) ages of 98.2 ± 0.6 Ma and 94.6 ± 1.4 Ma (J. E. Wright, personal

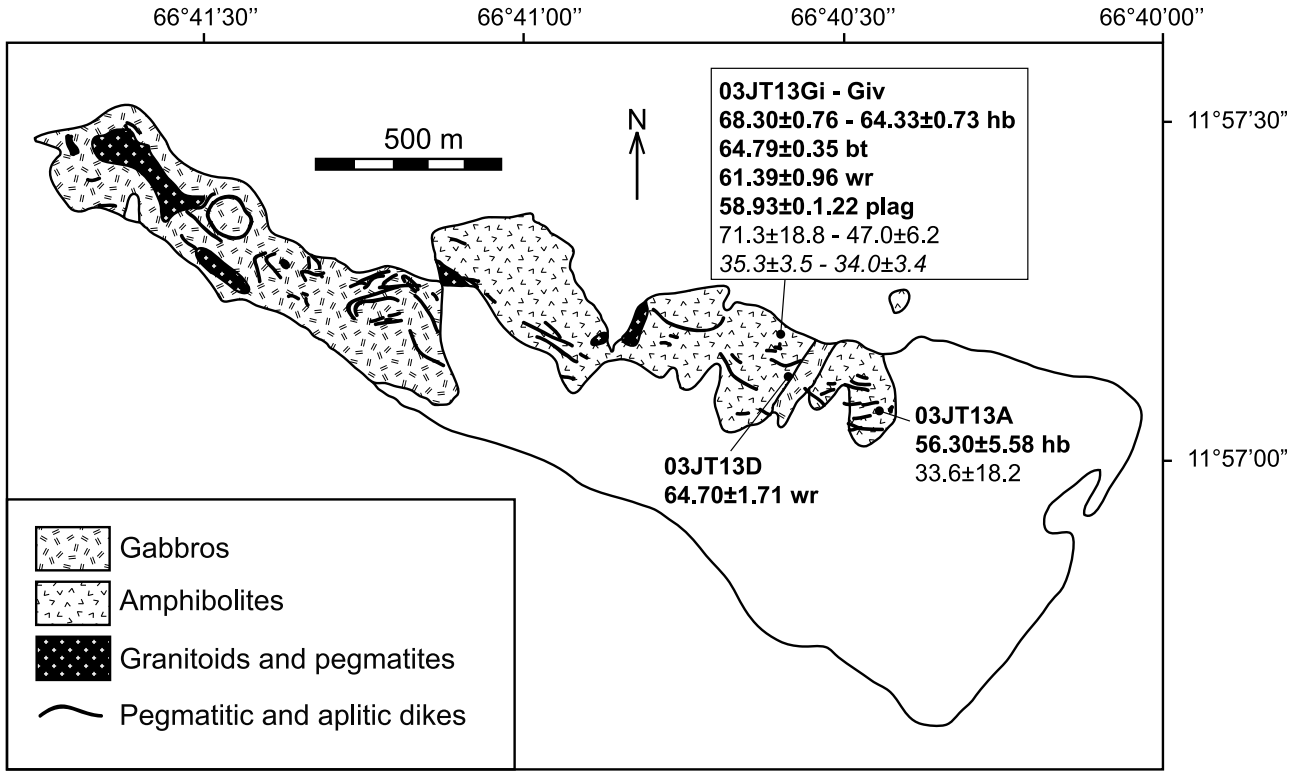

Figure 6. Geological map of Gran Roque, simplified after *Aguerrevere and López* [1938]. Sample locations and codes are shown, including $^{40}Ar/^{39}Ar$ ages (Ma ± 2σ in bold text: hb, hornblende; bt, biotite; gm, glass free groundmass; plag, plagioclase), apatite fission track ages (Ma ± 2σ in normal text), and apatite (U-Th)/He ages (Ma ± 2σ in italic text).

communication, 2008) are the most reliable radiometric ages for the rhyolites. The stratigraphic juxtaposition of the paleontological and U/Pb zircon ages defines a stratigraphic upward younging sequence, suggesting that all of these ages may be valid. The ~100–85 Ma age, combined with an island arc geochemical signature [*Beets et al.*, 1977], suggests the Washikemba Formation was not constructed on a 91–88 Ma Caribbean Plateau, and probably originated in an intraoceanic arc [*Thompson et al.*, 2004].

[16] After tilting, the Washikemba Formation was unconformably overlain by the Rincon Formation [*Beets et al.*, 1977] (Figure 5), which contains granodioritic clasts that resemble the plutonic rocks on Aruba [*Pijpers*, 1933]. The Rincon Formation was previously determined to be Maastrichtian [*Beets et al.*, 1977], but if the identification of the fossils in this sedimentary unit, including pseudorbitoides, is correct [*Beets et al.*, 1977], then the Rincon Formation may be Middle to Late Campanian [*Mitchell and Ramsook*, 2009]. The Southern Complex is unconformably overlain by the Soebi Blanco fluvial conglomerate, which contains numerous continental-derived gneissic and granitic clasts. Some of these clasts have been dated by U/Pb (zircon) at ~1150 Ma [*Priem et al.*, 1986b] and may be derived from the basement of the Guajira Peninsula, 300 km to the west [*Priem et al.*, 1986b; *Molina et al.*, 2006] (Figure 2). Similar material may be found in Danian turbidites on the neighboring island of Curaçao [*Beets et al.*, 1977]. The exact age of the Soebi Blanco Formation is not known, although its age range is bracketed by incorporated Campanian-Maastrichtian limestone clasts and unconformably overlying upper Eocene sedimentary rocks [*Beets et al.*, 1977]. The Miocene-Pliocene Seroe Domi Formation is widespread in the central part of the island.

2.2.3. Gran Roque

[17] The oldest rocks on Gran Roque are amphibolites (Figure 6), which are derived from either MORB [*Santamaría and Schubert*, 1974; *Ostos and Sisson*, 2005] or oceanic plateau rocks [*Giunta et al.*, 2002], and crystallized at 130 ± 14 Ma (K/Ar [*Santamaría and Schubert*, 1974]). These are intruded by gabbros which were later metamorphosed to lower greenschist facies. Undeformed quartz diorites, pegmatites and aplites of island arc affinity [*Santamaría and Schubert*, 1974; *Giunta et al.*, 2002; *Ostos and Sisson*, 2005] extensively intruded the amphibolites and gabbros (Figure 6) at 65 ± 3.6 Ma (K/Ar [*Santamaría and Schubert*, 1974]). The only exposed sedimentary cover on Gran Roque is Quaternary.

3. Analytical Methods

3.1. SIMS U-Th-Pb Zircon

[18] Zircon grains were separated from the rock samples, mounted in epoxy resin, polished to approximately half-grain thickness, imaged by a variety of techniques (cath-

Table 1. Ion Micro-Probe U-Pb Zircon Data[a]

Sample Spot	U (ppm)	Th (ppm)	Pb (ppm)	Th/U	f^{206} (%)	$^{238}U/^{206}Pb \pm \sigma\%$	$^{207}Pb/^{206}Pb$ Age $\pm \sigma\%$	$^{206}Pb/^{238}U$ (Ma) $\pm \sigma$
3	148	78	2	0.527	0.53	74.007 ± 1.16	0.04926 ± 2.9	86.5 ± 1.0
4	52	18	1	0.352	1.23	74.668 ± 1.10	0.05182 ± 5.0	85.8 ± 0.9
5[b]	47	12	1	0.254	1.99	70.239 ± 1.32	0.05765 ± 6.1	91.1 ± 1.2
6	48	10	1	0.214	0.7	71.829 ± 1.49	0.04640 ± 5.0	89.1 ± 1.3
7	75	17	1	0.232	1.19	74.132 ± 1.30	0.05144 ± 4.0	86.4 ± 1.1
9	112	45	2	0.404	0.51	72.101 ± 1.04	0.04685 ± 3.3	88.8 ± 0.9
10[b]	67	19	1	0.280	1.56	75.071 ± 0.79	0.05401 ± 4.0	85.3 ± 0.7
13	142	57	2	0.404	0.62	73.267 ± 1.33	0.04697 ± 3.1	87.4 ± 1.2
15[b]	74	22	1	0.296	1.04	75.526 ± 1.03	0.05365 ± 3.9	84.8 ± 0.9
18	43	10	1	0.230	2.43	76.166 ± 1.33	0.05168 ± 5.1	84.1 ± 1.1
22	117	47	2	0.399	0.81	72.819 ± 1.23	0.04945 ± 3.2	87.9 ± 1.1
20	58	15	1	0.251	0.74	75.552 ± 1.17	0.05106 ± 4.4	84.8 ± 1.0
24	60	14	1	0.242	1.09	72.639 ± 1.19	0.04569 ± 4.9	88.1 ± 1.0
26	94	33	1	0.356	0.62	73.217 ± 0.95	0.04691 ± 3.4	87.4 ± 0.8

[a]Here f^{206} (%) is the percentage of common ^{206}Pb, estimated from the measured ^{204}Pb. All errors are at the 1σ level. Age calculations use the routines of *Ludwig* [2003] and follow the decay constant recommendations of *Steiger and Jäger* [1977]. Tonalite ARU94-18 was sampled near Alta Vista Chapel, Aruba.

[b]Analyses are excluded from the final Concordia age calculation.

odoluminescence (CL), secondary electron, backscatter electrons (BSD), transmitted and reflected light) and analyzed using the Nordsim Cameca IMS1270 ion microprobe at the Swedish Museum of Natural History, Stockholm. Operating conditions for the instrument were routine [e.g., *Whitehouse and Kamber*, 2005], namely an ~15 μm analytical spot size, primary beam current of 5–10 nA at –13 kV (total energy 23 kV) which illuminated a 150 μm aperture and a mass resolution of 4500. After 120 s of presputtering to remove the gold coating, beam centering, mass calibration and energy adjustments were performed automatically and 12 cycles through the mass stations were used for data collection. Correction of isotope ratios for common Pb was based on the measured ^{204}Pb (corrected for average background) and is considered to represent surface laboratory contamination [e.g., *Zeck and Whitehouse*, 1999]. Common Pb correction uses an assumed present-day average crustal composition [*Stacey and Kramers*, 1975]. Isotope ratios and corresponding ages (calculated using standard decay constants) are listed in Table 1 together with 1σ uncertainties. All ages discussed in the text are given at 2σ uncertainties. U/Pb calibration is based on repeat analysis of 91500 zircon and uses a best fit power law relationship between Pb/U and UO_2/U for each analytical session. Phanerozoic aged crystals have generally more reliable $^{206}Pb/^{238}U$ ages than $^{207}Pb/^{206}Pb$ ages as error magnification on low count rates of ^{207}Pb increases rapidly towards younger times. However, $^{206}Pb/^{238}U$ ages are dependent on the appropriateness of the U/Pb calibration as determined from repeat analysis of the standard throughout the analytical session. The UO_x/U value of the unknowns is within the range defined by the standards and there is no indication of matrix matching effects. Within run ratios were examined and for zircon rim analyses confirm that homogeneous material was sampled throughout the ablation depth.

3.2. The $^{40}Ar/^{39}Ar$ Analysis

[19] Hand-picked, unaltered hornblende and biotite separates from the Aruba Batholith and Gran Roque were rinsed in deionized water and 5% HNO_3 in an ultrasonic bath, packed in copper foil and irradiated in the CLICIT facility of the TRIGA reactor at Oregon State University for 15 h. Samples were degassed by CO_2-IR laser step heating, and the extracted gas was gettered in a stainless steel UHV line, after passing through a cold trap chilled to ~150 Kelvin. Argon isotopes were analyzed using a GV Instruments Argus mass spectrometer equipped with four high-gain (1E12 ohms) Faraday detectors, and a single 1E11 ohm Faraday detector (^{40}Ar). Data reduction was performed using the ArArCALC software [*Koppers*, 2002]. Experimental details are presented by *Marschik et al.* [2008]. The data are presented in Table 2.

3.3. Apatite Fission Track Analysis

[20] Whole rock samples were crushed and apatite was recovered using conventional heavy liquid and magnetic methods. Apatite grains were mounted in epoxy, polished and etched using 5.5M HNO_3 for 20 s at 21.0 ± 0.5°C in a temperature-calibrated water bath. Apatite fission track data were obtained using the external detector method [*Gleadow*, 1981]. Maximum etch pit diameters were used to assess the intergrain variation of annealing kinetics in samples from Aruba and Bonaire (Dpar [*Carlson et al.*, 1999]). Similar information was obtained from apatites extracted from Gran Roque by determining their chlorine content. Further details are provided in the appendix, and data are presented in Table 3.

3.4. (U-Th)/He Analysis

3.4.1. Samples From Aruba and Bonaire

[21] Prismatic, inclusion free apatite grains were measured with a Leica polarizing stereomicroscope and individually packed in platinum microcrucibles. Helium was degassed from the apatites using a CO_2-IR laser at 1050°C, and the exact volume was determined using a quantitatively calibrated ^3He spike on a Balzers quadrupole mass spectrometer at the University of Lausanne, Switzerland. A second degassing step was performed to determine if the apatites

Table 2. The $^{40}Ar/^{39}Ar$ CO_2-IR Laser Step-Heating Data for the Aruba Batholith and Crystalline Rocks on Gran Roque[a]

	^{36}Ar (a)	^{37}Ar (Ca)	^{38}Ar (Cl)	^{39}Ar (K)	$^{40}Ar^{b}$	$^{40}Ar^{b}$ Percent	^{39}Ar (K) Percent	K/Ca ± 2σ	Age ± 2σ
06VDL27 Hornblende (J = 0.0042432 ± 0.0000085)[c]									
Step 1	0.000183	0.000264	0.000000	0.000252	0	0.00	0.06	0.410 ± 2.620	0.00 ± 0.00
Step 2	0.001162	0.003939	0.000000	0.001818	0	0.00	0.40	0.198 ± 0.069	0.00 ± 0.00
Step 3	0.001540	0.229765	0.000156	0.016277	0.246364602	35.13	3.59	0.030 ± 0.002	112.29 ± 5.72
Step 4	0.001342	0.344696	0.000195	0.021981	0.255145043	39.14	4.84	0.027 ± 0.002	86.74 ± 4.07
Step 5	0.000945	0.377883	0.000284	0.023360	0.307897077	52.44	5.15	0.027 ± 0.002	98.18 ± 3.26
Step 6	0.001812	0.786468	0.000726	0.043622	0.530964195	49.79	9.61	0.024 ± 0.002	90.85 ± 1.90
Step 7	0.002285	0.986812	0.000886	0.056464	0.673374064	49.93	12.44	0.025 ± 0.002	89.06 ± 1.38
Step 8	0.002784	1.379244	0.001111	0.077515	0.932754033	53.13	17.08	0.024 ± 0.002	89.84 ± 1.21
Step 9	0.003349	2.073749	0.001755	0.113920	1.384356327	58.31	25.11	0.024 ± 0.002	90.71 ± 1.07
Step 10	0.002015	1.664099	0.001596	0.088120	1.047008402	63.75	19.42	0.023 ± 0.002	88.74 ± 1.18
Step 11	0.000144	0.176911	0.000112	0.010395	0.121118433	74.02	2.29	0.025 ± 0.002	87.06 ± 6.18
Weighted plateau							85.96	0.024 ± 0.001	89.76 ± 0.85
06VDL05 Hornblende (J = 0.0042385 ± 0.0000085)[d]									
Step 1	0.000263	0.002176	0.000000	0.000459	0	0.00	0.07	0.091 ± 0.035	0.00 ± 0.00
Step 2	0.000414	0.002773	0.000000	0.001265	0.00965046	7.31	0.18	0.196 ± 0.082	57.41 ± 48.01
Step 3	0.001049	0.002793	0.000000	0.003086	0	0.00	0.44	0.475 ± 0.176	0.00 ± 0.00
Step 4	0.001330	0.005602	0.000000	0.005459	0.033994183	7.96	0.79	0.419 ± 0.096	47.00 ± 14.40
Step 5	0.002723	0.190304	0.000252	0.024321	0.269705835	25.10	3.50	0.055 ± 0.004	82.87 ± 2.77
Step 6	0.002246	0.338094	0.000300	0.034159	0.378904621	36.34	4.91	0.043 ± 0.003	82.88 ± 2.08
Step 7	0.002312	0.575803	0.000511	0.052521	0.622127766	47.66	7.56	0.039 ± 0.003	88.38 ± 1.66
Step 8	0.001365	0.437618	0.000470	0.038688	0.495352035	55.12	5.57	0.038 ± 0.003	95.34 ± 1.94
Step 9	0.000747	0.212150	0.000180	0.020830	0.256328396	53.74	3.00	0.042 ± 0.003	91.72 ± 3.71
Step 10	0.001648	0.404007	0.000347	0.037442	0.441275817	47.53	5.39	0.040 ± 0.003	87.94 ± 2.34
Step 11	0.001493	0.401086	0.000480	0.033505	0.407078497	47.99	4.82	0.036 ± 0.002	90.59 ± 2.09
Step 12	0.001707	0.533493	0.000464	0.044397	0.532658716	51.37	6.39	0.036 ± 0.002	89.48 ± 1.65
Step 13	0.001638	0.527819	0.000476	0.041907	0.485080733	50.05	6.03	0.034 ± 0.002	86.41 ± 1.83
Step 14	0.002385	0.702701	0.000626	0.053946	0.673142699	48.85	7.76	0.033 ± 0.002	92.98 ± 1.24
Step 15	0.002433	0.797557	0.000788	0.059191	0.691928784	49.04	8.52	0.032 ± 0.002	87.24 ± 1.54
Step 16	0.002262	0.945491	0.000931	0.071810	0.83566229	55.55	10.33	0.033 ± 0.002	86.86 ± 1.31
Step 17	0.001835	1.178013	0.001229	0.079747	0.989904457	64.60	11.47	0.029 ± 0.002	92.50 ± 1.03
Step 18	0.001362	1.223111	0.001239	0.084670	1.061352903	72.51	12.18	0.030 ± 0.002	93.39 ± 1.20
Step 19	0.000355	0.060428	0.000078	0.007652	0.104803002	50.00	1.10	0.054 ± 0.004	101.80 ± 8.53
Weighted mean age							89.01	0.034 ± 0.002	90.61 ± 1.74
06VDL05 Biotite (J = 0.0042291 ± 0.0000085)									
Step 1	0.002883	0.000638	0.000005	0.011854	0.019222399	2.21	0.24	7.984 ± 19.131	12.33 ± 11.84
Step 2	0.002233	0.000879	0.000051	0.024942	0.131098893	16.58	0.51	12.195 ± 17.108	39.66 ± 5.28
Step 3	0.002784	0.001144	0.000153	0.094552	0.403169802	32.88	1.92	35.551 ± 45.214	32.24 ± 1.29
Step 4	0.003800	0.000000	0.000452	0.245627	1.305207396	53.75	4.98	0.015 ± 0.000	40.09 ± 0.54
Step 5	0.006712	0.001179	0.000730	0.523763	3.769214578	65.52	10.62	191.094 ± 195.910	54.09 ± 0.27
Step 6	0.008264	0.002273	0.000771	0.592224	5.09947681	67.61	12.01	112.042 ± 56.271	64.53 ± 0.24
Step 7	0.008141	0.012466	0.000831	0.644754	6.330706864	72.46	13.08	22.239 ± 2.638	73.40 ± 0.20
Step 8	0.008070	0.017101	0.000752	0.650785	6.792750478	74.01	13.20	16.364 ± 1.905	77.93 ± 0.23
Step 9	0.006038	0.019093	0.000596	0.544596	5.894891117	76.76	11.04	12.265 ± 1.127	80.75 ± 0.19
Step 10	0.004765	0.015903	0.000630	0.496416	5.442998792	79.44	10.07	13.423 ± 1.705	81.77 ± 0.21
Step 11	0.003557	0.012068	0.000520	0.391530	4.31678735	80.41	7.94	13.951 ± 2.197	82.22 ± 0.30
Step 12	0.003802	0.011642	0.000489	0.402090	4.452355981	79.84	8.15	14.851 ± 2.005	82.56 ± 0.29
Step 13	0.002640	0.003542	0.000400	0.268794	3.026682421	79.50	5.45	32.627 ± 14.569	83.93 ± 0.49
Step 14	0.000452	0.000000	0.000042	0.039139	0.431185892	76.36	0.79	0.003 ± 0.000	82.15 ± 3.69
Total fusion age									71.91 ± 0.30
03JT13A Hornblende (J = 0.0048590 ± 0.0000097)[e]									
Step 1	0.000133	0.001747	0.000035	0.000261	0.011866	23.21	0.42	0.064 ± 0.022	360.11 ± 285.91
Step 2	0.000314	0.005941	0.000011	0.000746	0.022736	19.66	1.19	0.054 ± 0.005	249.28 ± 116.32
Step 3	0.000321	0.012389	0.000000	0.000703	0.015704	14.22	1.13	0.024 ± 0.003	185.79 ± 213.57
Step 4	0.000261	0.049797	0.000051	0.000838	0.027917	26.59	1.34	0.007 ± 0.001	270.77 ± 153.13
Step 5	0.000300	0.227274	0.000002	0.003249	0.035655	28.65	5.21	0.006 ± 0.000	93.73 ± 42.71
Step 6	0.000446	0.901026	0.000029	0.013692	0.094222	41.69	21.94	0.007 ± 0.000	59.34 ± 7.33
Step 7	0.000632	1.396544	0.000086	0.024039	0.141404	43.10	38.52	0.007 ± 0.000	50.84 ± 5.23
Step 8	0.000516	0.977475	0.000005	0.016187	0.114249	42.81	25.94	0.007 ± 0.000	60.83 ± 5.99
Step 9	0.000424	0.119642	0.000000	0.002684	0.014874	10.61	4.30	0.010 ± 0.000	47.93 ± 60.55
Weighted mean age							95.92	0.007 ± 0.001	56.30 ± 5.58
03JT13D Whole Rock (J = 0.0048070 ± 0.0000096)[f]									
Step 1	0.002190	0.132178	0.000090	0.005221	0.003374	0.52	1.36	0.017 ± 0.001	5.60 ± 23.83
Step 2	0.001112	0.435331	0.000000	0.008755	0.000000	0.00	2.28	0.009 ± 0.000	0.00 ± 0.00
Step 3	0.000658	0.761192	0.000000	0.013478	0.119069	37.97	3.52	0.008 ± 0.000	75.03 ± 12.18

Table 2. (continued)

	^{36}Ar (a)	^{37}Ar (Ca)	^{38}Ar (Cl)	^{39}Ar (K)	^{40}Ar^{b}	^{40}Ar^{b} Percent	^{39}Ar (K) Percent	K/Ca ± 2σ	Age ± 2σ
Step 4	0.000407	1.290899	0.000000	0.012887	0.095596	44.28	3.36	0.004 ± 0.000	63.21 ± 9.74
Step 5	0.000551	2.500258	0.000000	0.026256	0.189958	53.83	6.85	0.005 ± 0.000	61.67 ± 5.71
Step 6	0.000677	4.204508	0.000005	0.050889	0.431016	68.29	13.28	0.005 ± 0.000	72.00 ± 3.20
Step 7	0.000758	5.136586	0.000000	0.059210	0.402931	64.27	15.45	0.005 ± 0.000	58.07 ± 3.06
Step 8	0.000559	4.682596	0.000122	0.054090	0.415398	71.54	14.12	0.005 ± 0.000	65.40 ± 3.36
Step 9	0.000643	4.785981	0.000000	0.055279	0.403801	67.99	14.43	0.005 ± 0.000	62.26 ± 3.08
Step 10	0.000375	3.411169	0.000057	0.039246	0.307337	73.51	10.24	0.005 ± 0.000	66.67 ± 3.43
Step 11	0.000280	2.139098	0.000000	0.022912	0.174795	67.85	5.98	0.005 ± 0.000	64.98 ± 6.07
Step 12	0.000376	2.623250	0.000015	0.028405	0.217287	66.17	7.41	0.005 ± 0.000	65.15 ± 4.49
Step 13	0.000048	0.652352	0.000000	0.006567	0.073550	83.87	1.71	0.004 ± 0.000	94.60 ± 15.04
Weighted plateau							52.18	0.005 ± 0.000	64.70 ± 1.71
				03JT13Gi Whole Rock (J = 0.0048420 ± 0.0000097)[g]					
Step 1	0.007220	0.348034	0.000000	0.011451	0.077757	3.52	1.55	0.014 ± 0.001	58.36 ± 12.40
Step 2	0.001280	0.456995	0.000000	0.018523	0.070787	15.76	2.51	0.017 ± 0.001	33.08 ± 4.46
Step 3	0.000812	0.842606	0.000213	0.024381	0.237471	49.73	3.30	0.012 ± 0.001	83.14 ± 3.76
Step 4	0.000683	1.413384	0.000000	0.032446	0.287038	58.70	4.40	0.010 ± 0.000	75.67 ± 3.75
Step 5	0.000582	1.765275	0.000000	0.043190	0.307424	64.11	5.85	0.011 ± 0.000	61.13 ± 3.96
Step 6	0.000490	1.935618	0.000000	0.053143	0.381191	72.48	7.20	0.012 ± 0.000	61.59 ± 3.23
Step 7	0.002138	9.653558	0.000000	0.286658	2.012235	76.09	38.85	0.013 ± 0.001	60.30 ± 1.15
Step 8	0.000564	3.075128	0.000000	0.092123	0.670400	80.09	12.48	0.013 ± 0.001	62.47 ± 1.63
Step 9	0.000625	3.419796	0.000000	0.102092	0.741560	80.06	13.84	0.013 ± 0.001	62.36 ± 1.74
Step 10	0.000079	0.506859	0.000028	0.016211	0.128946	84.74	2.20	0.014 ± 0.001	68.18 ± 10.52
Step 11	0.000170	0.708023	0.000000	0.021870	0.160344	76.12	2.96	0.013 ± 0.001	62.94 ± 6.88
Step 12	0.000156	0.875875	0.000000	0.026266	0.215670	82.34	3.56	0.013 ± 0.001	70.34 ± 4.94
Step 13	0.000039	0.342591	0.000014	0.009541	0.086537	88.18	1.29	0.012 ± 0.000	77.54 ± 11.40
Weighted plateau							83.38	0.012 ± 0.001	61.39 ± 0.96
				03JT13Gii Hornblende (J = 0.0048560 ± 0.0000097)[h]					
Step 1	0.000499	0.005432	0.000000	0.001918	0.044684	23.26	0.22	0.152 ± 0.066	193.34 ± 59.99
Step 2	0.002555	0.013543	0.000009	0.005566	0.134999	15.17	0.63	0.177 ± 0.032	200.87 ± 25.83
Step 3	0.002841	0.024264	0.000038	0.004777	0.113680	11.93	0.54	0.085 ± 0.011	197.28 ± 28.70
Step 4	0.003420	0.047370	0.000025	0.004996	0.150906	12.99	0.57	0.045 ± 0.005	246.93 ± 20.25
Step 5	0.001843	0.109993	0.000066	0.007417	0.093389	14.64	0.84	0.029 ± 0.002	107.07 ± 11.22
Step 6	0.003853	0.562133	0.000486	0.032255	0.360959	24.07	3.66	0.025 ± 0.002	95.47 ± 3.85
Step 7	0.000146	0.021913	0.000000	0.001228	0.023821	35.52	0.14	0.024 ± 0.004	162.41 ± 90.51
Step 8	0.004491	3.276087	0.002036	0.173396	1.445577	52.13	19.68	0.023 ± 0.002	71.60 ± 1.13
Step 9	0.001032	1.477876	0.000963	0.082605	0.696224	69.54	9.38	0.024 ± 0.002	72.37 ± 1.48
Step 10	0.001574	2.604066	0.001767	0.140818	1.125883	70.76	15.99	0.023 ± 0.002	68.72 ± 1.37
Step 11	0.001119	3.666858	0.002554	0.201255	1.598519	82.86	22.85	0.024 ± 0.002	68.28 ± 1.23
Step 12	0.000724	2.002624	0.001200	0.108456	0.856859	80.00	12.31	0.023 ± 0.002	67.92 ± 1.72
Step 13	0.000530	1.419833	0.001016	0.079831	0.629700	80.09	9.06	0.024 ± 0.002	67.81 ± 1.69
Step 14	0.000331	0.668839	0.000453	0.036349	0.294175	75.02	4.13	0.023 ± 0.002	69.54 ± 3.86
Weighted plateau							64.34	0.024 ± 0.001	68.30 ± 0.76
				03JT13Gii Plagioclase (J = 0.0048210 ± 0.0000096)[i]					
Step 1	0.005900	0.200751	0.000021	0.013911	0.188859	9.77	3.53	0.030 ± 0.003	114.38 ± 9.00
Step 2	0.006033	0.876096	0.000000	0.040863	0.285962	13.82	10.38	0.020 ± 0.002	59.86 ± 2.70
Step 3	0.002405	1.042542	0.000000	0.044361	0.337212	32.18	11.27	0.018 ± 0.002	64.93 ± 2.77
Step 4	0.004712	2.459846	0.000000	0.107997	0.745133	34.86	27.43	0.019 ± 0.002	59.03 ± 1.87
Step 5	0.003252	1.872938	0.000000	0.068401	0.480309	33.33	17.38	0.016 ± 0.002	60.06 ± 2.49
Step 6	0.001895	1.243539	0.000000	0.037487	0.259231	31.64	9.52	0.013 ± 0.001	59.16 ± 3.96
Step 7	0.001482	1.102795	0.000000	0.030738	0.208143	32.22	7.81	0.012 ± 0.001	57.95 ± 4.44
Step 8	0.000759	0.724136	0.000000	0.018251	0.127661	36.29	4.64	0.011 ± 0.001	59.83 ± 5.74
Step 9	0.000428	0.413601	0.000000	0.008797	0.053039	29.55	2.23	0.009 ± 0.001	51.69 ± 8.20
Step 10	0.000515	0.506563	0.000000	0.022847	0.154674	50.39	5.80	0.019 ± 0.002	57.94 ± 3.27
Weighted plateau							74.82	0.012 ± 0.003	58.93 ± 1.22
				03JT13Giii Hornblende (J = 0.0048520 ± 0.0000097)[j]					
Step 1	0.004141	0.058545	0.000017	0.012513	0.083773	6.41	0.39	0.092 ± 0.004	57.67 ± 12.83
Step 2	0.002425	0.073061	0.000105	0.017713	0.210024	22.66	0.56	0.104 ± 0.004	100.91 ± 8.80
Step 3	0.002129	0.076912	0.000137	0.020280	0.151355	19.39	0.64	0.113 ± 0.005	64.17 ± 6.14
Step 4	0.002002	0.190779	0.000521	0.041979	0.335357	36.18	1.32	0.095 ± 0.004	68.61 ± 2.78
Step 5	0.001421	0.430086	0.000924	0.069233	0.516555	55.15	2.18	0.069 ± 0.003	64.16 ± 1.58
Step 6	0.002812	1.900222	0.004768	0.198495	1.566237	65.33	6.25	0.045 ± 0.002	67.78 ± 0.73
Step 7	0.002990	4.416965	0.011021	0.389729	3.023462	77.38	12.27	0.038 ± 0.001	66.66 ± 0.47
Step 8	0.002531	5.291713	0.013461	0.459883	3.521558	82.48	14.48	0.037 ± 0.001	65.81 ± 0.46
Step 9	0.001481	3.432376	0.008245	0.301204	2.234441	83.61	9.48	0.038 ± 0.001	63.79 ± 0.50
Step 10	0.001297	4.030743	0.010262	0.361032	2.714970	87.62	11.37	0.039 ± 0.001	64.65 ± 0.49

Table 2. (continued)

	^{36}Ar (a)	^{37}Ar (Ca)	^{38}Ar (Cl)	^{39}Ar (K)	^{40}Ar^{b}	^{40}Ar^{b} Percent	^{39}Ar (K) Percent	K/Ca ± 2σ	Age ± 2σ
Step 11	0.001955	4.692214	0.011355	0.415595	3.056736	84.10	13.08	0.038 ± 0.001	63.26 ± 0.50
Step 12	0.001477	4.528956	0.011425	0.396306	2.995392	87.27	12.48	0.038 ± 0.001	64.98 ± 0.46
Step 13	0.000923	2.604057	0.006597	0.246550	1.863768	87.23	7.76	0.041 ± 0.002	64.99 ± 0.57
Step 14	0.000576	1.581157	0.003892	0.149538	1.170474	87.29	4.71	0.041 ± 0.002	67.25 ± 1.09
Step 15	0.000484	0.934528	0.002242	0.096128	0.741311	83.81	3.03	0.044 ± 0.002	66.27 ± 1.45
Weighted mean age							54.17	0.038 ± 0.001	64.33 ± 0.73
				03JT13Giii Biotite (J = 0.0048490 ± 0.0000097)[k]					
Step 1	0.000395	0.001922	0.000083	0.017003	0.054555	31.87	0.33	3.805 ± 0.642	27.85 ± 5.96
Step 2	0.000353	0.001693	0.000060	0.029619	0.168953	61.83	0.57	7.523 ± 1.253	49.22 ± 4.01
Step 3	0.000350	0.001645	0.000153	0.054373	0.377035	78.46	1.05	14.210 ± 2.577	59.66 ± 2.15
Step 4	0.000453	0.002570	0.000283	0.139651	1.006898	88.26	2.70	23.362 ± 3.178	62.00 ± 1.05
Step 5	0.000470	0.002699	0.000117	0.183978	1.318106	90.45	3.56	29.308 ± 4.332	61.61 ± 1.02
Step 6	0.000459	0.003055	0.000511	0.224440	1.634863	92.33	4.34	31.596 ± 3.653	62.62 ± 0.82
Step 7	0.000356	0.005231	0.000394	0.244144	1.795092	94.45	4.72	20.068 ± 1.403	63.20 ± 0.82
Step 8	0.000636	0.007726	0.001282	0.588524	4.369195	95.86	11.38	32.755 ± 1.865	63.80 ± 0.35
Step 9	0.000336	0.002887	0.000486	0.201315	1.505666	93.80	3.89	29.986 ± 3.893	64.27 ± 0.89
Step 10	0.000358	0.006393	0.000587	0.320193	2.411423	95.78	6.19	21.536 ± 1.388	64.71 ± 0.50
Step 11	0.000179	0.006388	0.000612	0.306788	2.345457	97.78	5.93	20.650 ± 1.476	65.67 ± 0.41
Step 12	0.000156	0.003156	0.000417	0.207867	1.579064	97.15	4.02	28.322 ± 3.279	65.26 ± 0.88
Step 13	0.000285	0.016704	0.000806	0.371869	2.798124	97.07	7.19	9.573 ± 0.401	64.65 ± 0.43
Step 14	0.000169	0.004695	0.000404	0.172681	1.309125	96.31	3.34	15.814 ± 1.159	65.13 ± 0.89
Step 15	0.000169	0.006787	0.000580	0.253235	1.931790	97.47	4.90	16.044 ± 0.884	65.53 ± 0.76
Step 16	0.000982	0.058939	0.003574	1.854994	13.970237	97.95	35.88	13.533 ± 0.509	64.71 ± 0.23
Weighted plateau							55.32	12.031 ± 2.896	64.79 ± 0.35
				03JT13Giv Hornblende (J = 0.0048530 ± 0.0000097)[l]					
Step 1	0.003815	0.021150	0.000048	0.003400	0.128584	10.24	0.33	0.069 ± 0.007	303.99 ± 37.80
Step 2	0.001518	0.025327	0.000035	0.002843	0.061447	12.05	0.28	0.048 ± 0.006	179.93 ± 38.02
Step 3	0.002686	0.072465	0.000004	0.006268	0.130461	14.11	0.62	0.037 ± 0.003	173.61 ± 19.74
Step 4	0.003212	0.112087	0.000076	0.007610	0.149767	13.63	0.75	0.029 ± 0.002	164.56 ± 18.17
Step 5	0.003178	0.123013	0.000114	0.009751	0.144175	13.31	0.96	0.034 ± 0.002	125.02 ± 15.71
Step 6	0.004696	0.323580	0.000456	0.024865	0.293763	17.47	2.44	0.033 ± 0.002	100.58 ± 5.63
Step 7	0.003710	0.770806	0.001386	0.056945	0.504261	31.50	5.59	0.032 ± 0.002	75.91 ± 2.46
Step 8	0.004073	1.717027	0.003242	0.128962	1.066780	46.99	12.66	0.032 ± 0.002	71.01 ± 1.33
Step 9	0.004762	2.998399	0.005929	0.226826	1.885601	57.26	22.26	0.033 ± 0.002	71.35 ± 0.96
Step 10	0.003748	2.931375	0.005615	0.217014	1.775725	61.58	21.30	0.032 ± 0.002	70.25 ± 0.98
Step 11	0.002063	2.077989	0.004204	0.155642	1.214071	66.57	15.28	0.032 ± 0.002	67.03 ± 1.13
Step 12	0.001220	1.181191	0.002328	0.088195	0.696511	65.89	8.66	0.032 ± 0.002	67.85 ± 1.36
Step 13	0.000628	0.835498	0.001477	0.059329	0.465943	71.52	5.82	0.031 ± 0.002	67.48 ± 2.00
Step 14	0.000372	0.433550	0.000643	0.031269	0.244338	68.94	3.07	0.031 ± 0.002	67.15 ± 3.81
Weighted mean age							32.82	0.031 ± 0.001	67.38 ± 0.82

[a]Data are baseline and blank corrected and are corrected for postirradiation decay of ^{37}Ar (T0.5 = 35.1 days) and ^{39}Ar (T0.5 = 269 years). Mass discrimination value during analyses was 0.99786 ± 0.5%. Correction factors for interfering isotopes have been calculated from 10 analyses of two Ca-glass samples and 22 analyses of two pure K glass samples and are ^{36}Ar/^{37}Ar(Ca) = 2.603E-4 ± 2.373E-9, ^{39}Ar/^{37}Ar(Ca) = 6.501E-4 ± 7.433E-9, and ^{40}Ar/^{39}Ar(K) = 1.547E-2 ± 7.455E-7.
[b]Radiogenic ^{40}Ar.
[c]Steps 6–11 were used to calculate the weighted plateau values.
[d]Steps 7–18 were used to calculate the weighted mean age values.
[e]Steps 5–9 were used to calculate the weighted mean age values.
[f]Steps 8–12 were used to calculate the weighted plateau values.
[g]Steps 5–11 were used to calculate the weighted plateau values.
[h]Steps 10–14 were used to calculate the weighted plateau values.
[i]Steps 4–10 were used to calculate the weighted plateau values.
[j]Steps 9–13 were used to calculate the weighted mean age values.
[k]Steps 12–16 were used to calculate the weighted plateau values.
[l]Steps 11–14 were used to calculate the weighted mean age values.

enclosed any remaining He due to high U inclusions [*Farley and Stockli*, 2002]. The apatites were subsequently dissolved in $HNO_{3(aq)}$ spiked with known amounts of ^{235}U and ^{230}Th, and U and Th concentrations were measured on a Perkin-Elmer quadrupole ICP-MS. Raw ages were calculated using custom-made software. The consistency of the analytical equipment was regularly monitored by analyzing crystals of Durango fluorapatite, with a known age of 31.4 ± 0.5 Ma [*Solé and Pi*, 2005]. Analytical error is estimated to be no higher than 10% (2σ) and lower than the scatter caused by fluid inclusions or variable diffusivity of individual grains [e.g., *Fitzgerald et al.*, 2006]. The data are presented in Table 4.

Table 3. Apatite Fission Track Data for Aruba, Bonaire, and Gran Roque[a]

	UTM EAST	UTM NORTH	Alt. (m)	Grains Counted	ρD ($\times10^5$ cm^{-2})	ρs ($\times10^5$ cm^{-2})	ρi ($\times10^5$ cm^{-2})	DPar (μm)	P(X^2) (%)	U (ppm)	Pooled FT Age (Ma) ± 2σ	Mean Length (μm) ± 1σ	Length SD (μm)
Aruba													
06VDL01	385643	1394760	10	8	14.3285 (6698)	7.430 (133)	23.464 (420)	ND	78.2	25.8	85.2 ± 17.4		
06VDL05	390494	1390849	3	21	14.0177 (6698)	10.276 (484)	33.036 (1556)	2.19	70.3	34.6	82.0 ± 9.4	11.8 ± 0.3 (81)	2.9
06VDL06	391624	1389734	3	6	13.8623 (6698)	7.237 (110)	25.789 (392)	2.47	52.3	22.9	73.2 ± 16.2	13.6 ± 0.2 (72)	1.9
06VDL08	387825	1392401	7	10	13.7068 (6698)	6.747 (168)	22.249 (554)	2.58	95.3	25.9	78.2 ± 14.4	13.5 ± 0.3 (50)	2.0
06VDL11	391216	1388738	41	8	13.3960 (6698)	26.505 (273)	112.136 (1155)	1.975	34.5	99.1	59.6 ± 8.6	12.7 ± 0.3 (78)	2.2
06VDL16	393869	1387224	20	25	12.9297 (6698)	3.610 (235)	13.871 (903)	2.02	16.3	17.9	62.5 ± 9.6	13.3 ± 0.1 (98)	1.3
06VDL18	392446	1385601	48	29	12.7743 (6698)	3.000 (480)	11.469 (1835)	1.9	65.6	12	62.9 ± 7.2	13.6 ± 0.3 (77)	1.4
06VDL25	395953	1382858	65	12	12.0464 (5729)	19.209 (413)	67.907 (1460)	1.65	42.4	81.5	64.2 ± 7.9	13.2 ± 0.1 (119)	1.2
06VDL27	396813	1382461	74	13	11.9157 (5729)	11.215 (323)	39.549 (1139)	ND	60.4	53	63.6 ± 8.6		
06VDL29	396056	1381276	40	14	11.7849 (5729)	3.449 (169)	11.714 (574)	ND	82.6	14.5	65.3 ± 12		
06VDL30	397600	1378458	54	5	11.6542 (5729)	20.533 (154)	87.600 (657)	ND	58.6	89	51.5 ± 9.6		
06VDL31	398784	1377392	37	6	11.5233 (5729)	5.229 (57)	22.385 (244)	ND	64.5	32	50.7 ± 15.2		
06VDL36	401326	1379058	51	4	11.2619 (5729)	1.500 (15)	4.100 (41)	ND	62.5	4	77.5 ± 47		
Bonaire													
06VDL48	564692	1359126	22	27	11.0003 (5729)	0.875 (49)	1.893 (106)	ND	98.6	2	95.5 ± 33.4		
06VDL49	566436	1358919	49	49	10.8659 (5729)	0.452 (66)	1.343 (196)	2.76	99.2	1.5	68.9 ± 19.9	13.2 ± 0.2 (80)	2.0
06VDL51	566517	1358423	93	74	10.7387 (5729)	0.695 (217)	1.671 (522)	ND	99.8	1.9	83.9 ± 14.2		
06VDL54	567880	1355994	90	23	13.8379 (6605)	0.469 (56)	1.264 (151)	3.24	82.8	1.1	96.4 ± 30.5	12.1 ± 0.3 (87)	2.6
06VDL62	564689	1351676	24	48	13.6095 (6605)	0.421 (74)	1.325 (233)	ND	99.3	1.1	81.3 ± 22.0		
06VDL64	580227	1347964	39	48	13.4954 (6605)	0.474 (77)	1.650 (268)	2.57	80.7	1.5	73 ± 19.2	12.3 ± 0.2 (114)	2.5

Gran Roque	UTM EAST	UTM NORTH	Alt. (m)	Grains Counted	ρD ($\times10^5$ cm^{-2})	ρs ($\times10^5$ cm^{-2})	ρi ($\times10^5$ cm^{-2})	Cl (wt %)	P(X^2) (%)	U (ppm)	Pooled FT Age (Ma) ± 2σ	Mean Length (μm) ± 1σ	Length SD (μm)
03JT13A	753285	1322234	10	2	7.65(3302)	7.78(17)	30.41(73)	ND	52.1	54.6	33.6 ± 18.2	14.6 ± 1.0(3)	1.7
03JT13Gii	753000	1322345	10	11	7.78(3302)	6.99(89)	14.39(183)	0.84–2.04	99.2	23.1	71.3 ± 18.8	14.7 ± 0.2(41)	1.4
03JT13Giii	753000	1322345	10	20	7.92(3302)	7.90(323)	24.02(982)	ND	77.4	37.9	49.1 ± 6.6	14.3 ± 0.1(100)	0.9
03JT13Giv	753000	1322345	10	20	9.53(3476)	10.28(337)	39.30(1288)	0.41–0.77	57.7	51.7	47.0 ± 6.2	14.4 ± 0.1(100)	1.1

[a]All fission track data from Aruba and Bonaire were acquired by R. van der Lelij with a zeta value of 378.4 ± 8.2 (apatite; CN5 standard glass). All fission track data from Gran Roque were acquired by Matthias Raab (University of Melbourne, Australia) with a zeta value of 378.8 ± 5.5 (apatite; CN5 standard glass). Values in parentheses are quantity of tracks.

Table 4. Apatite (U-Th)/He Data From Aruba, Bonaire, and Gran Roque[a]

	Mean Radius (μm)	Length (μm)	He (mol)	^{238}U (mol)	^{235}U (mol)	^{232}Th (mol)	U (ppm)	Th (ppm)	FT Factor	Raw Age (Ma)	FT Corr. Age ± 10% (Ma)
06VDL05 Aruba											
Aliquot 1	60	161	1.34E-14	2.87E-13	2.11E-15	5.63E-13	16.0	30.4	0.77	19.0	25.2 ± 2.5
Aliquot 2	46	154	2.25E-15	4.94E-14	3.63E-16	3.89E-13	4.6	35.2	0.71	8.9	**13.4 ± 1.3**
Aliquot 3	46	182	1.88E-15	4.95E-14	3.63E-16	3.96E-13	3.8	29.2	0.72	7.5	**11.3 ± 1.1**
Mean											12.4 ± 1.2
06VDL11 Aruba											
Aliquot 1	56	154	5.74E-15	1.30E-13	9.54E-16	5.01E-13	6.4	24.0	0.73	13.2	18.1 ± 1.8
Aliquot 2	56	175	3.91E-15	1.29E-13	9.45E-16	4.47E-13	5.6	18.9	0.73	9.5	**13.0 ± 1.3**
Aliquot 3	56	196	3.05E-15	1.13E-13	8.28E-16	4.99E-13	7.1	30.4	0.73	7.6	**10.4 ± 1.0**
Mean											11.7 ± 1.2
06VDL18 Aruba											
Aliquot 1	63	280	1.40E-14	2.87E-13	2.11E-15	6.87E-13	7.3	16.8	0.80	19.4	**25.4 ± 2.5**
Aliquot 2	60	154	1.45E-14	2.85E-13	2.09E-15	6.81E-13	16.8	38.9	0.77	19.6	**26.1 ± 2.6**
Aliquot 3	56	147	6.36E-15	1.83E-13	1.35E-15	5.74E-13	9.5	28.8	0.75	11.7	16.0 ± 1.6
Mean											25.8 ± 2.6
06VDL36 Aruba											
Aliquot 1	53	161	1.97E-15	6.33E-14	4.65E-16	4.10E-13	4.4	27.3	0.75	7.3	**10.3 ± 1.0**
Aliquot 2	67	154	3.06E-15	7.77E-14	5.71E-16	4.30E-13	2.7	14.6	0.78	10.4	13.5 ± 1.4
Aliquot 3	53	133	1.85E-15	1.00E-13	7.35E-16	4.26E-13	8.9	36.5	0.73	5.3	**7.4 ± 0.7**
Mean											8.9 ± 0.9
06VDL54 Bonaire											
Aliquot 1	49	168	9.67E-16	2.31E-14	1.70E-16	3.86E-13	2.2	36.3	0.73	4.9	**7.2 ± 0.7**
Aliquot 2	63	154	1.58E-15	6.74E-14	4.95E-16	5.18E-13	3.6	27.0	0.78	5.2	**6.9 ± 0.7**
Aliquot 3	49	175	6.48E-16	2.19E-14	1.61E-16	3.83E-13	1.2	21.1	0.74	3.5	5.2 ± 0.5
Mean											7.1 ± 0.7
06VDL64 Bonaire											
Aliquot 1	56	154	1.06E-15	1.53E-14	1.13E-16	3.60E-13	0.8	17.3	0.76	6.4	8.9 ± 0.9
Aliquot 2	49	140	7.94E-15	4.90E-14	3.60E-16	4.02E-13	3.5	27.7	0.72	31.2	45.6 ± 4.6
Aliquot 3	46	154	6.76E-16	3.79E-14	2.78E-16	3.97E-13	2.8	28.8	0.71	2.8	4.2 ± 0.4
Mean											ND

Table 4. (continued)

	Mean Radius (μm)	Number of Grains	He (mol)	Mass (mg)	U (ppm)	Th (ppm)	FT Factor	Raw Age (Ma)	FT Corr. Age ± 2σ (Ma)
03JT13Gii Gran Roque									
Aliquot 1	54	2	1.24E-14	0.0071	2.6	10.2	0.71	62.0	87.6 ± 8.8
Aliquot 2	42	2	1.03E-15	0.0057	2.3	5.8	0.67	8.9	13.3 ± 1.3
Aliquot 3	93	1	4.73E-14	0.0306	1.9	10.7	0.85	62.3	73.0 ± 7.3
Mean									ND
03JT13Giii Gran Roque									
Aliquot 1	63	2	7.27E-14	0.0121	27.7	44.6	0.77	28.7	**37.2 ± 3.7**
Aliquot 2	65	2	4.61E-14	0.0104	23.3	34.4	0.77	25.8	**33.4 ± 3.3**
Aliquot 3	82	2	1.07E-13	0.0351	19.6	31.0	0.83	20.7	24.9 ± 2.5
Mean									35.3 ± 3.5
03JT13Giv Gran Roque									
Aliquot 1	80	2	1.04E-13	0.0242	20.9	25.2	0.82	29.4	**35.7 ± 3.6**
Aliquot 2	75	2	1.01E-13	0.0203	26.7	32.2	0.80	26.5	**32.9 ± 3.3**
Aliquot 3	72	2	9.17E-14	0.0210	23.0	28.8	0.80	26.9	**33.5 ± 3.4**
Mean									34.0 ± 3.4

[a]Aliquots in bold type were used to calculate the mean ages. ND, no data.

3.4.2. Samples From Gran Roque

[22] He extraction was performed using a resistance furnace and He ratios were measured using a Balzers quadrupole mass spectrometer at the University of Melbourne, Australia. The apatites were subsequently dissolved in $HNO_{3(aq)}$ spiked with ^{229}Th and ^{233}U, and U and Th concentrations were measured on a Nu Plasma multicollector ICPMS.

4. Results

4.1. Aruba

[23] Eleven zircons, separated from one sample of the Aruba Batholith (Aru94-18) yielded a weighted mean, concordant U/Pb age of 87.00 ± 0.86 Ma (Figure 7). The error ellipses of individual grains are large due to low U contents of 43–150 ppm. Overall low lead resulted in a large scatter of ^{207}Pb/^{206}Pb ages.

[24] Two overlapping hornblende ^{40}Ar/^{39}Ar ages were obtained from the Aruba Batholith. Tonalite 06VDL27 yields a plateau age of 89.76 ± 0.85 Ma (Figure 8) spanning 86% of the total ^{39}Ar released, which is indistinguishable from its inverse isochron age of 301.7 ± 16.4 Ma. Tonalite 06VDL05 yields a discordant age spectrum with a weighted mean age of 90.61 ± 1.74 Ma over the flattest part of the age spectrum, which spans 89% of the total ^{39}Ar released. Partially chloritized biotite from sample 06VDL05 yields an age gradient between 32 and 84 Ma, suggesting that Argon has been partially lost (Figure 8).

[25] Thirteen samples of hornblende tonalite from the Aruba Batholith yield pooled apatite fission track ages ranging from 50.7 ± 15.2 Ma to 85.2 ± 8.7 Ma (Figure 3). P(χ^2) values are >5%, indicating that all fission track ages from any individual sample define a single fission track age population. Only one sample (06VDL05) initially had

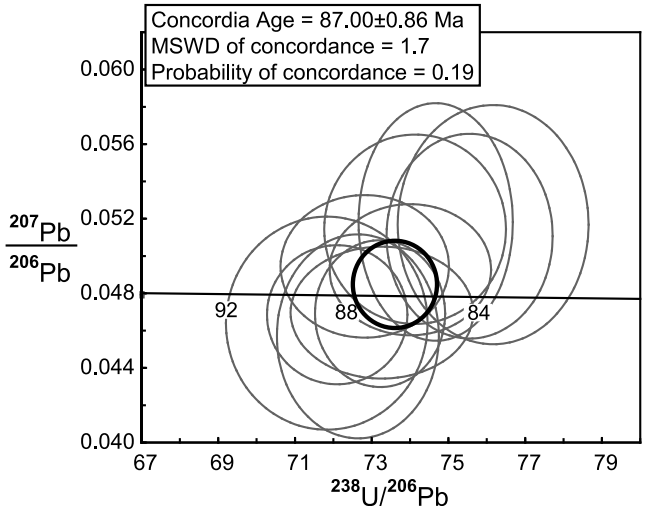

Figure 7. IMS zircon U/Pb results on a Tera-Wasserburg concordia plot for tonalite ARU94-18. Individual grain ages are shown as ellipses, and the weighted mean age is marked by a bold black circle. Error ellipses are ±2σ, and decay constant uncertainties are included.

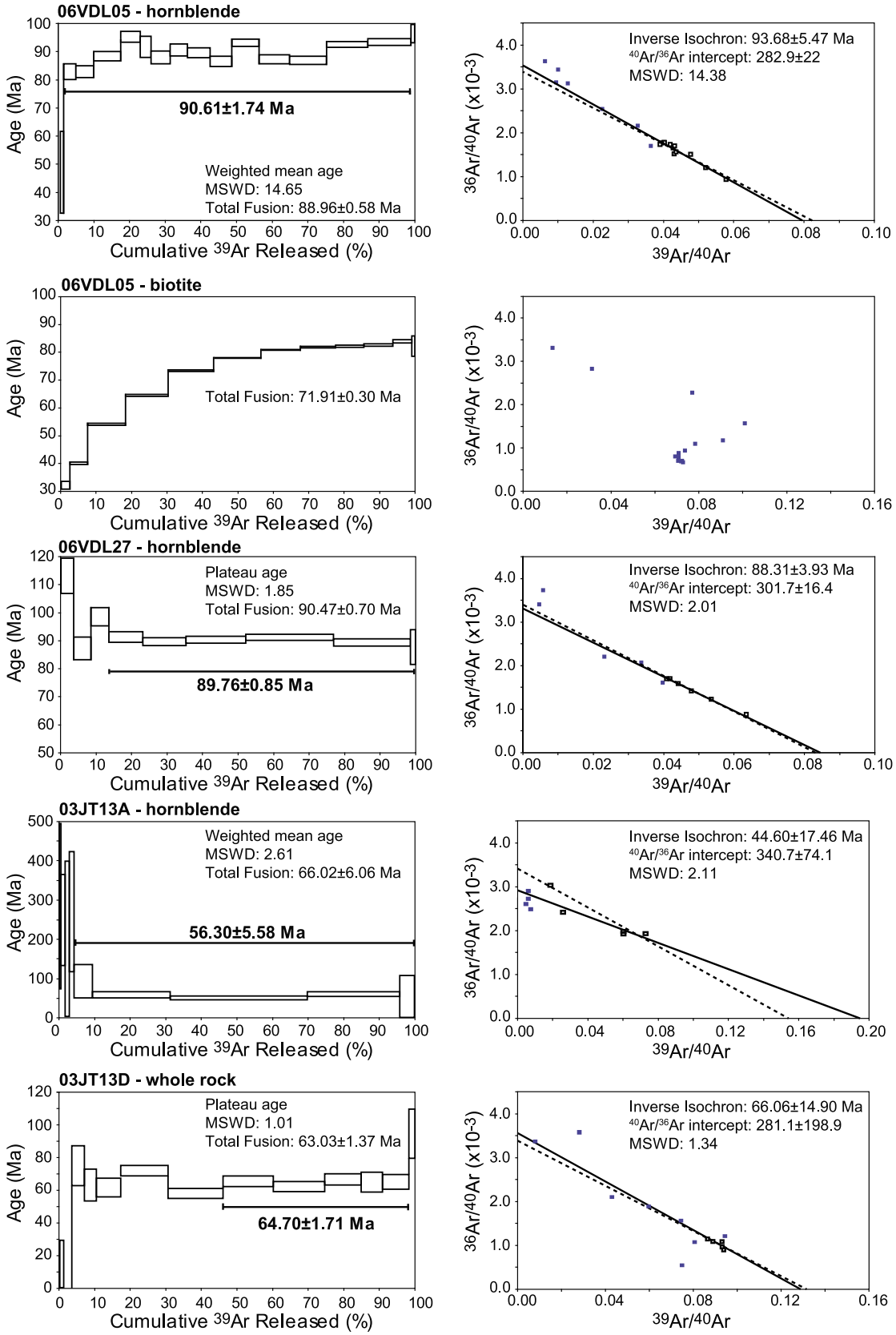

Figure 8. The $^{40}Ar/^{39}Ar$ age spectra and inverse isochron plots for the Aruba Batholith and crystalline rocks on Gran Roque. Errors are $\pm 2\sigma$.

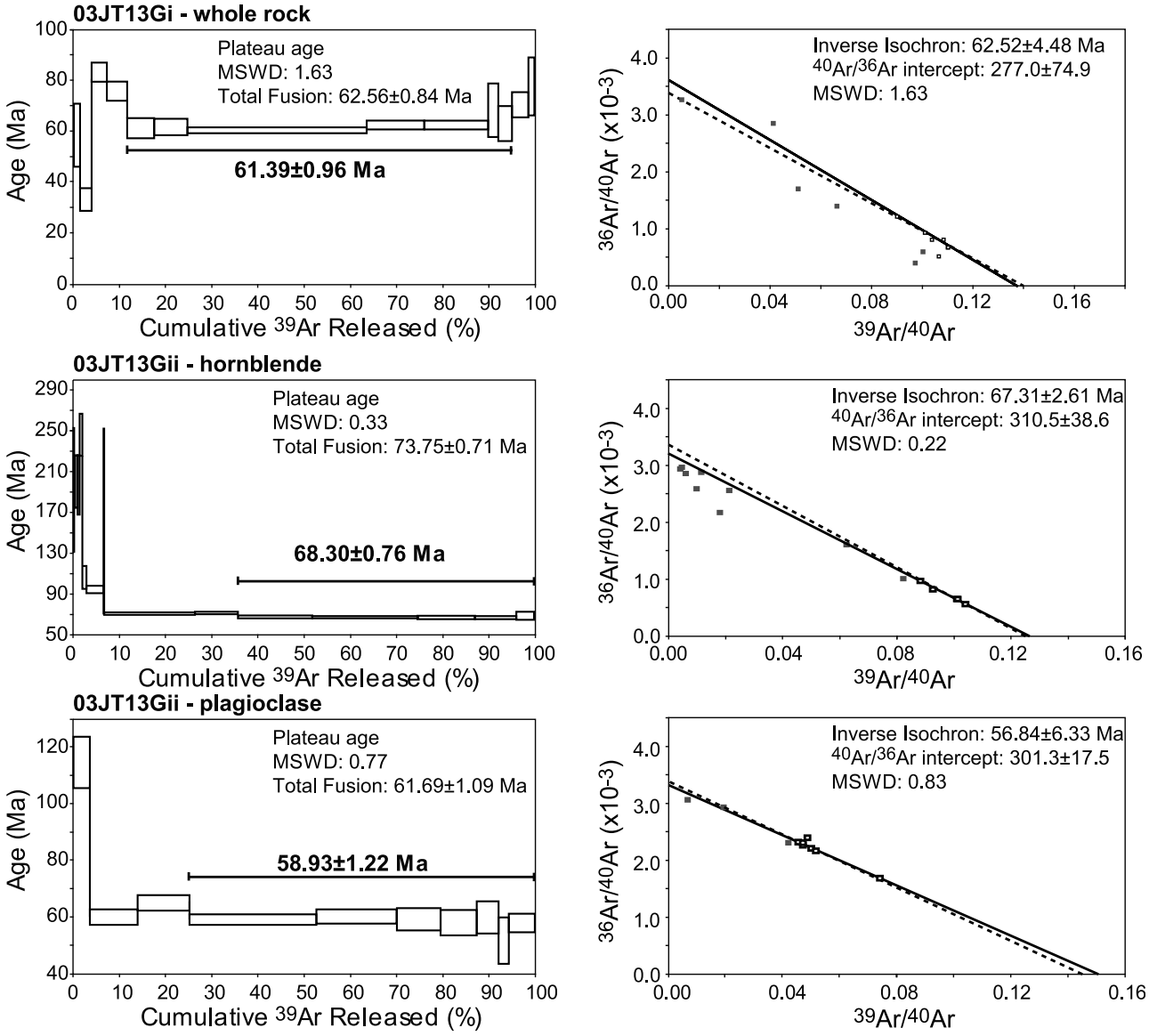

Figure 8. (continued)

sufficient measurable horizontal, confined tracks (≥40). Irradiation of the remaining apatite mounts with ^{252}Cf derived fission fragments enabled us to measure sufficient track lengths from six additional samples. Mean track lengths vary from 13.6 μm to 11.8 μm, and hence are partially annealed suggesting either prolonged residence in the apatite partial annealing zone during slow cooling, or reheating. The apatite fission track ages yield a NW-SE younging trend, although sufficient horizontal track lengths were only obtained from samples located in the central part of the batholith, rendering it difficult to interpret that trend.

[26] Four tonalites from the Aruba Batholith yielded similar (U-Th)/He ages from individual aliquots, and mean ages which span between 25.8 ± 2.6 Ma and 7.1 ± 0.7 Ma (Figure 3). Aliquots which displayed evidence for the presence of high U inclusions (e.g., anomalously old ages or the presence of He in a second extraction of the same aliquot) were excluded from any interpretations. Some of the scatter in the data may result from the presence of tiny He-rich fluid inclusions that were too small to be detected during hand picking, but were observed in a majority of the etched apatites mounted for fission track analysis. Normally, such inclusions lead to ages which are too old [*Fitzgerald et al.*, 2006]. Individual grains also show variable U and Th content, which will result in variable accumulation of radiation damage and hence variations in He diffusivity [*Shuster and Farley*, 2009].

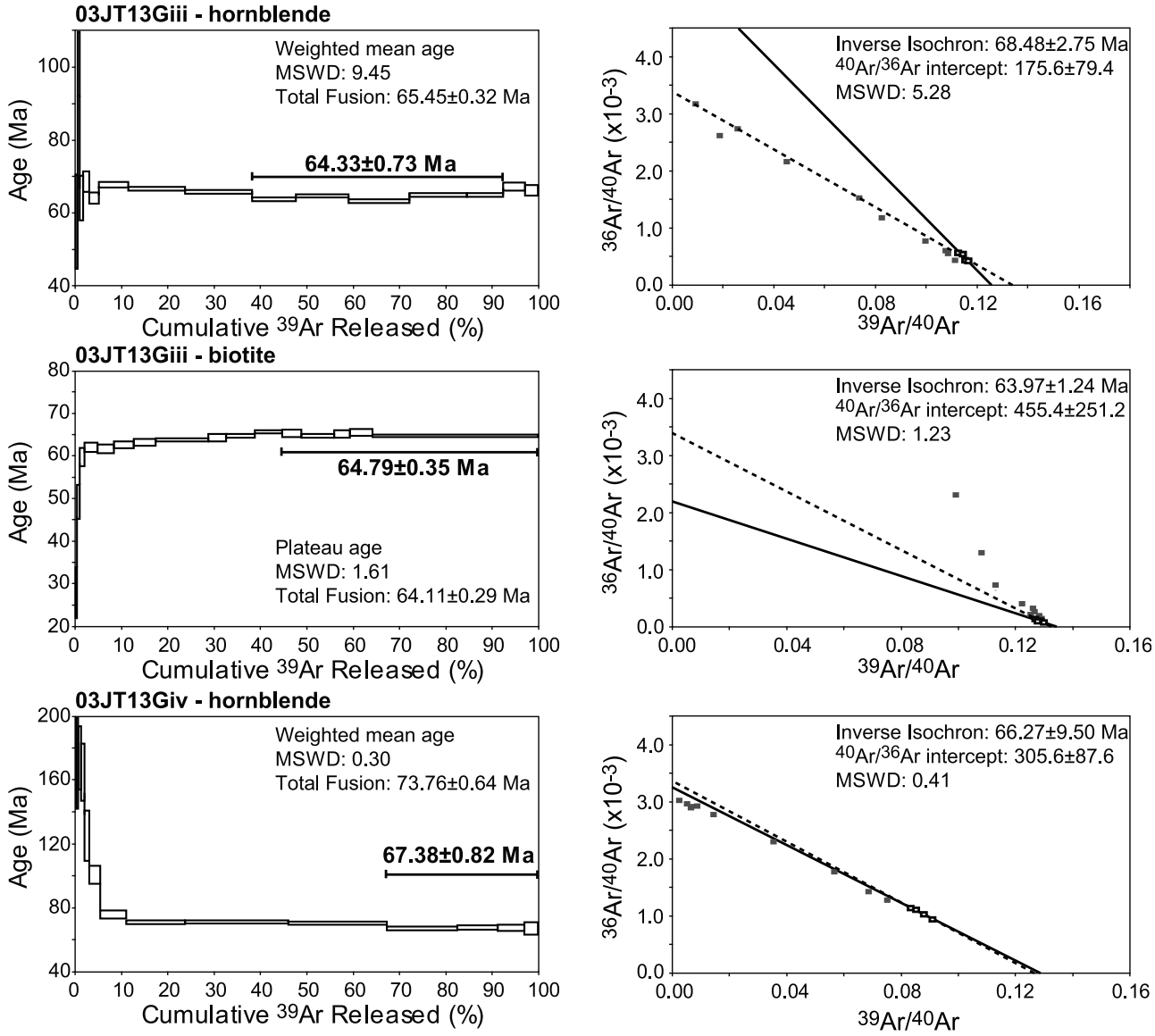

Figure 8. (continued)

4.2. Bonaire

[27] Apatites extracted from Albian to Coniacian rhyolites on Bonaire have very low U contents (<2 ppm), resulting in very low spontaneous fission track densities (Table 3). Consequently only six samples from the Washikemba Formation yielded useful apatite fission track ages, which range from 96.4 ± 30.5 to 68.9 ± 19.9 Ma (Figure 5), and the large errors preclude the identification of any spatial trend. Three samples from the Washikemba Formation yielded mean, confined track lengths that range from 13.2 to 12.1 μm, suggesting they are partially annealed. Due to abundant fluid inclusions and low U content, only one sample from the Northern Complex yielded a mean (U-Th)/He age of 6.7 ± 0.7 Ma. A sample from the Southern Complex yielded distinguishable ages from three different aliquots, and the data were discarded.

4.3. Gran Roque

[28] $^{40}Ar/^{39}Ar$ data were obtained from amphibolite-grade metabasic rocks and nonmetamorphosed quartz-dioritic dykes on Gran Roque (Figure 8). Hornblende from amphibolite-grade metadolerite 03JT13A yielded an imprecise, weighted mean age of 56.30 ± 5.58 Ma over the flattest part of the age spectrum. Amphibolite-grade metabasalt 03JT13D yielded a slightly older plateau age of 64.70 ± 1.37 Ma. Samples 03JT13Gi-Giv were collected from and close to an 8m thick, nonmetamorphosed quartz diorite dyke which intrudes into the amphibolites (Figure 6). A whole rock analysis of fine-grained amphibolite 03JT13Gi gave a plateau age of 61.39 ±

0.96 Ma, which is slightly younger than a hornblende plateau age of 68.30 ± 0.76 Ma obtained from amphibolite 03JT13Gii. Plagioclase extracted from 03JT13Gii yielded a plateau age of 58.93 ± 1.22 Ma. Hornblende from the quartz diorite dyke (03JT13Giii) gave a discordant age spectrum whose flattest portion has a weighted mean age of 64.33 ± 0.73 Ma, which overlaps with a plateau biotite age of 64.79 ± 0.35 Ma obtained from the same sample. Elevated ages in the initial heating steps of hornblende extracted from a second sample of the dyke (03JT13Giv) reveal the presence of excess ^{40}Ar, although the youngest flat portion of the age spectrum yields a weighted mean age of 67.38 ± 0.82 Ma, and an inverse isochron ^{40}Ar/^{36}Ar intercept which overlaps with the composition of atmospheric Ar.

[29] Apatites from Gran Roque host abundant dislocations, fluid inclusions and cracks, and fission track data were only acquired from four samples. Fine grained amphibolite 03JT13A yielded an unreliable pooled fission track age of 33.6 ± 18.2 Ma from two grains of poor quality. Amphibolite 03JT13Gii gave a pooled fission track age of 71.3 ± 18.8 Ma from eleven grains which have a large variation in Cl content (0.84–2.04 Wt %; Table 3). Twenty high-quality grains from quartz diorite 03JT13Giii yielded a fission track age of 49.1 ± 6.6 Ma. An indistinguishable age of 47.0 ± 6.2 was obtained from quartz diorite 03JT13Giv. Mean track lengths range between 14.3 and 14.7 μm, suggesting that the samples have experienced less annealing than the samples from Aruba and Bonaire.

[30] Quartz diorites 03JT13Giii and 03JT13Giv gave indistinguishable apatite (U-Th)/He, weighted mean ages of 35.3 ± 3.5 Ma and 34.0 ± 3.4 Ma, respectively, calculated from aliquot ages that are indistinguishable, suggesting the ages are accurate and are not influenced by heterogeneously dispersed, high-U inclusions.

5. Interpretation

5.1. Crystallization Age of the Aruba Batholith

[31] All published zircon U/Pb and hornblende ^{40}Ar/^{39}Ar plateau ages obtained from the Aruba Batholith span between ~90 Ma to ~87 Ma. No evidence for sufficiently large-scale structural displacement can be found in the batholith [e.g., *Beets et al.*, 1996], and geochemical analyses of several samples of the Aruba Batholith yield the same result [*White et al.*, 1999], suggesting that the batholith grew via several magmatic pulses emplaced into the same region over a time span of ~3 Ma. This interpretation provides a baseline within which the lower-temperature thermochronological data have been interpreted.

[32] The oldest reliable ages from the Aruba Batholith are a hornblende ^{40}Ar/^{39}Ar plateau age of 89.76 ± 0.85 Ma (this study) and a SHRIMP-RG U/Pb zircon age of 89 ± 1 Ma from a geographically adjacent sample [*Wright and Wyld*, 2004; J. E. Wright, personal communication, 2008]. These ages render the early phases of batholith intrusion indistinguishable from the age of ammonite fauna recovered from the Aruba Lava Formation [*MacDonald*, 1968; *Wiedmann*, 1978]. The short time available for the transition from surface exposure to batholith emplacement depth led *Wright and Wyld* [2004] to suggest the Aruba Lava Formation was partially subducted prior to batholith intrusion. The ~90 Ma ages for the Aruba Batholith are similar to zircon U/Pb ages obtained from the Buga Granite in Colombia (91.5 ± 1.3 Ma and 90.6 ± 1.2 Ma; Figure 1 [*Villagómez et al.*, 2008]) and the Pujilí Granite in Ecuador (85.5 ± 1.2 Ma; Figure 1 [*Vallejo et al.*, 2006, 2009]) which also intrude ~90 Ma oceanic plateau rocks, suggesting that the mechanism responsible for the petrogenesis of these tonalites may have been widespread and related to activity at the same plate boundary.

[33] Biotite crystals extracted from tonalites of the Aruba Batholith frequently reveal the presence of chloritized rims, accounting for the partial ^{40}Ar loss profile yielded by biotites extracted from 06VDL05.

5.2. Crystallization Age of Intrusions on Gran Roque

[34] All concordant plateau ^{40}Ar/^{39}Ar ages obtained from the unmetamorphosed quartz diorites and their host amphibolitic sequences span between 68.30 ± 0.76 Ma and 58.93 ± 1.22 Ma (Figure 8). The oldest hornblende ages of 67.38 ± 0.82 Ma (03JT13Giv) and 68.30 ± 0.76 Ma (03JT13Gii) are indistinguishable and were obtained from a nonmetamorphosed quartz diorite dyke and an amphibolite located less than ten meters from the dyke, respectively. The nonmetamorphosed nature of the dyke suggests the amphibolites were reset by contact metamorphism, and the ages indicate the time of cooling through 550°C–500°C, and probably represent a reasonable approximation of the age of the dyke, supporting the suggestion of *Santamaría and Schubert* [1974]. The biotite ^{40}Ar/^{39}Ar age yielded by the quartz diorite dyke (03JT13Giii) of 64.79 ± 0.35 Ma indicates the time that central Gran Roque cooled through 350°C–300°C, representing a high average cooling rate of 65°C/Myr during 68–65 Ma. Such a high cooling rate reflects thermal relaxation of the dyke and its aureole, subsequent to retrogression of the amphibolitic host rocks, which commenced at an undetermined time. The younger plagioclase and groundmass ^{40}Ar/^{39}Ar ages of 61–59 Ma obtained from amphibolites within several meters of the dyke reveal the time of cooling through 300°C–200°C, suggesting that cooling rates drastically decelerated during the Paleocene. Finally, the more regionally dispersed samples within the southeastern part of Gran Roque (Figure 6) yielded imprecise whole rock and hornblende ^{40}Ar/^{39}Ar ages from amphibolites between 65 and 56 Ma, which we interpret to reflect cooling subsequent to resetting by contact metamorphism during dyke emplacement.

5.3. Thermal Histories of Crystalline Rocks on the Leeward Antilles

[35] Crystalline magmatic rocks exposed on the Leeward Antilles have resided in the apatite partial annealing zone, and been periodically reheated because (1) the fission tracks in apatite are partially annealed, and (2) a majority of sedimentary rocks were deposited prior to the ages recorded by the (U-Th)/He data. We have utilized the controlled random search procedure provided by the HeFTy program [*Ketcham*, 2005] to search for solutions that simultaneously satisfy (1) apatite fission track age and track length dis-

tributions and (2) apatite (U-Th)/He data from single samples. The numerical solutions utilized the apatite fission track annealing model of *Ketcham et al.* [1999] and we applied c axis projected track lengths to account for variations caused by anisotropic annealing [e.g., *Donelick*, 1991; *Donelick et al.*, 1999]. Annealing kinetics and initial track lengths for all grains from which track length data were obtained from Aruba and Bonaire were evaluated using maximum etch pit diameters (Dpar) according to the model of *Carlson et al.* [1999]. Annealing kinetics and initial track lengths for samples from Gran Roque were evaluated using Cl contents according to the model of *Carlson et al.* [1999]. Helium diffusion in apatite was modeled using the algorithm of *Flowers et al.* [2009], which accounts for variable helium retentivity in apatite as a function of radiation damage. We assumed that U and Th parent isotopes were homogeneously distributed, He has only been ejected from apatite by recoil or diffusion and no He has been implanted by high-U neighbors.

[36] Thermal history solutions for Aruba were forced to commence at temperatures >200°C, with an oldest possible starting time of 90 Ma. The same constraint was forced onto the thermal history solutions for Bonaire because post-Washikemba Formation prehnite-pumpellyite facies metamorphism requires reheating to at least 200°C [*Philpotts*, 1990] after eruption, thus resetting all low-temperature thermochronometers after the late Turonian–early Coniacian sedimentary sequences were buried. One sample from the Southern Complex (06VDL64) was sampled directly below an unconformable contact with the Paleogene Soebi Blanco Formation, and we therefore forced the path from this sample to reach <30°C in the Paleogene. Two samples from Gran Roque (03JT13Giii and 03JT13Giv) yielded thermochronological data that can be used to generate sensible thermal history models. The thermal history solutions were forced to commence at temperatures >200°C, with an oldest possible starting time of 70 Ma, representing the time of dyke intrusions and high-temperature thermal overprinting. Sample 03JT13Gii was considered unsuitable for modeling because the chlorine composition of the apatites is extremely varied and falls outside the composition range of the samples on which apatite annealing characteristics were initially determined [see *Carlson et al.*, 1999], and the apatite fission track age (71.3 ± 18.8 Ma) is older than the plagioclase $^{40}Ar/^{39}Ar$ age (58.93 ± 1.22 Ma) obtained from the same sample.

5.4. Periods of Heating and Cooling

5.4.1. Aruba

[37] With the exception of 06VDL05, all modeled samples from Aruba reveal an initial phase of rapid cooling from at least ~120°C to below ~40°C (Figure 9) in the Late Cretaceous–early Paleocene. The timing of cooling varies between samples, with the most precise models (06VDL11, 16, 18, 25) yielding cooling through their respective apatite partial annealing zones between ~70 Ma and ~60 Ma, at rates of ~20°C/Myr. As a consequence of poor analytical precision, samples 06VDL06 and 06VDL08 yield less precise "acceptable" fit envelopes that nevertheless overlap onto the best fit paths of the more precise models. No good fits were found for sample 06VDL05 and the "acceptable" fit envelope is considered to be a loose approximation of the thermal history of the sample.

[38] The thermal history solutions require cooling from a minimum temperature of 50°C–40°C since the middle to late Miocene to obtain acceptable fits to both the apatite fission track and (U-Th)/He data. This is not clear in the thermal history envelopes because uncertainties in the timing of maximum temperatures in the Neogene permit acceptable fits to overlap each other, graphically masking the minimum required temperatures. The maximum temperature for the present surface of Aruba during the middle to late Miocene was ~60°C. All time-temperature models generated with (U-Th)/He data reveal a period of heating of 20°C between the Eocene and the middle to late Miocene.

5.4.2. Bonaire

[39] Thermal history solutions for all three modeled samples from the Northern and Southern complexes of the Washikemba Formation are very similar. Acceptable fit envelopes are very large due to the large age uncertainties, but the near perfect overlap of best fit solutions from the three samples reveals two main phases of cooling: (1) cooling of >80°C between 90 and 80 Ma at rates of ~8°C/Myr and (2) cooling of 80°C–60°C between 55 and 50 Ma at rates of ~5°C/Myr. The (U-Th)/He data yielded by sample 06VDL54, located in the center of the Northern Complex, requires a third phase of cooling of 40°C–30°C in the late Miocene, at rates of ~3°C/Myr. This model only found "acceptable" thermal history solutions, perhaps because its apatite fission track age is relatively old with a large uncertainty (96.4 ± 30.5), which is difficult to reconcile in models with the available track length data, (U-Th)/He age and posteruption low-temperature metamorphism.

5.4.3. Gran Roque

[40] Both modeled samples from Gran Roque yielded very similar thermal history solutions (Figure 9) with an initial phase of rapid cooling of >80°C at ~50 Ma, at rates >10°C/Myr. A second phase of cooling of 40°C–20°C may have initiated in the middle to late Miocene at rates of >3°C/Myr.

6. Tectonic Evolution of the Leeward Antilles

6.1. Tectonic and Paleogeographic Origin of Aruba, Bonaire, and Gran Roque

[41] Numerous similarities in the isotopic, geochemical, geochronological and paleomagnetic data published for the Caribbean Plate and the Piñon and Pallatanga terranes [*Luzieux et al.*, 2006; *Vallejo et al.*, 2006] (Figure 1) exposed in the Western Cordillera and external fore arc of Ecuador lead us to favor an allochthonous model for the Caribbean Plate, suggesting it originated in the Pacific region. Consequently, our interpretations of data collected from the Bonaire Block will take into account the allochthonous nature of its basement sequence.

[42] The Aruba Lava Formation erupted in the Turonian (93.6 ± 0.8 to 88.6 Ma), yields typical oceanic plateau geochemical signatures and is commonly considered to represent a detached remnant of the CCOP [e.g., *White et*

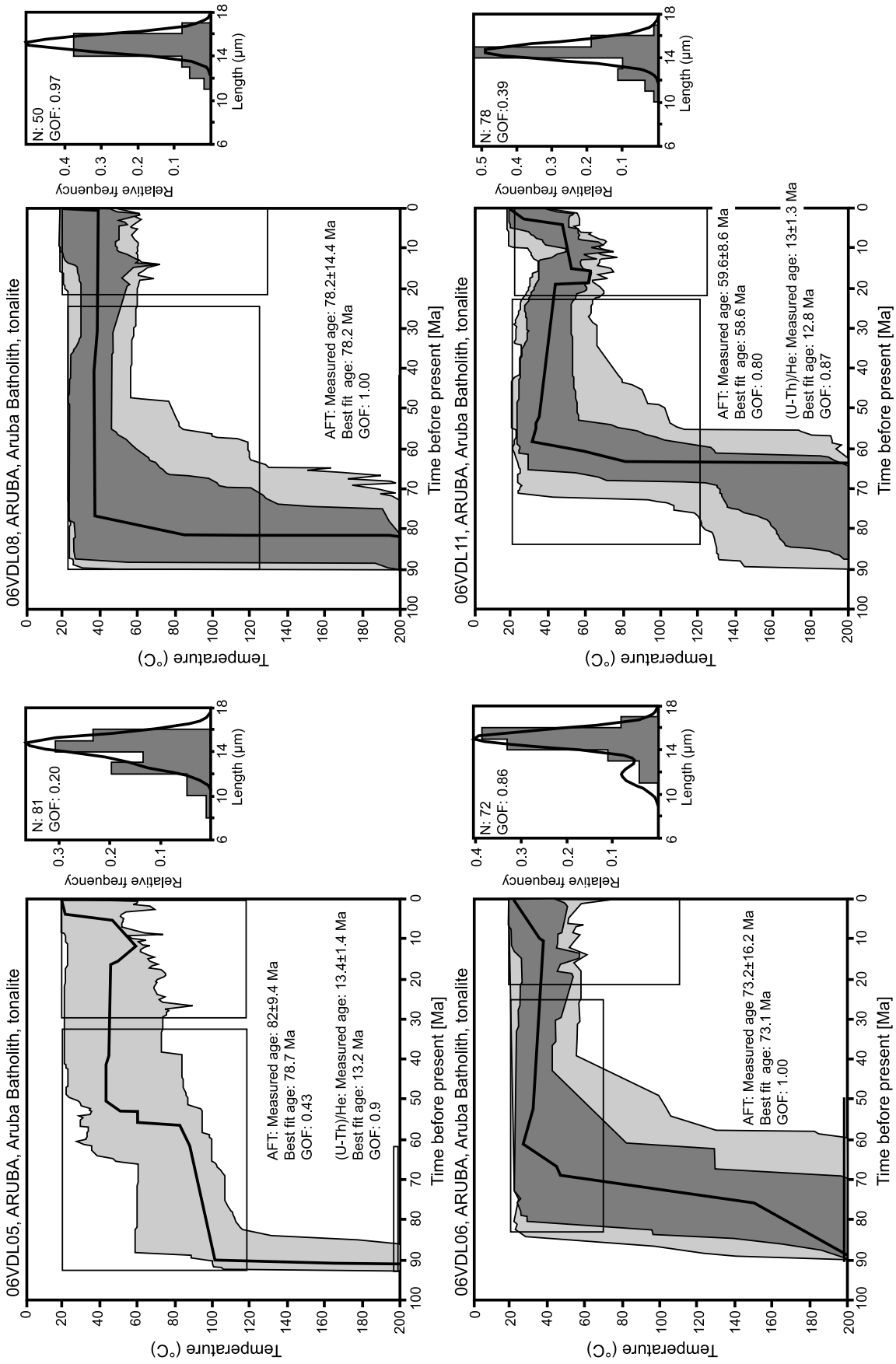

Figure 9. Time-temperature paths for all modeled samples from Aruba, Bonaire, and Gran Roque. Dark gray shaded areas are envelopes for "good fits," and light gray shaded areas are envelopes for "acceptable fits." The bold line shows the statistically best fitting solution. The solutions were considered to be good fits when track length histograms and model ages passed the Kuiper's statistic test with values of >0.5 and acceptable with values of >0.05. GOF, goodness-of-fit.

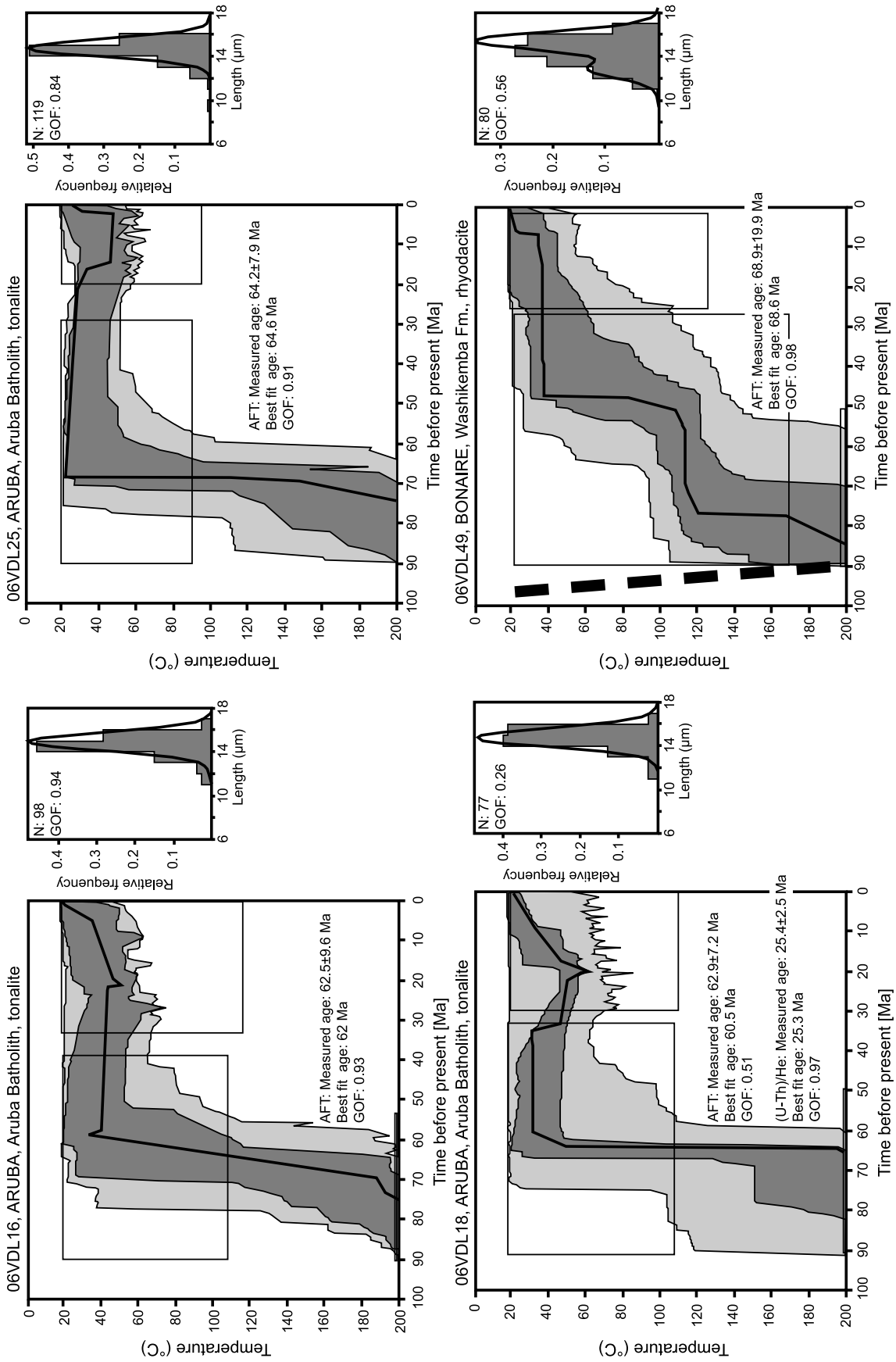

Figure 9. (continued)

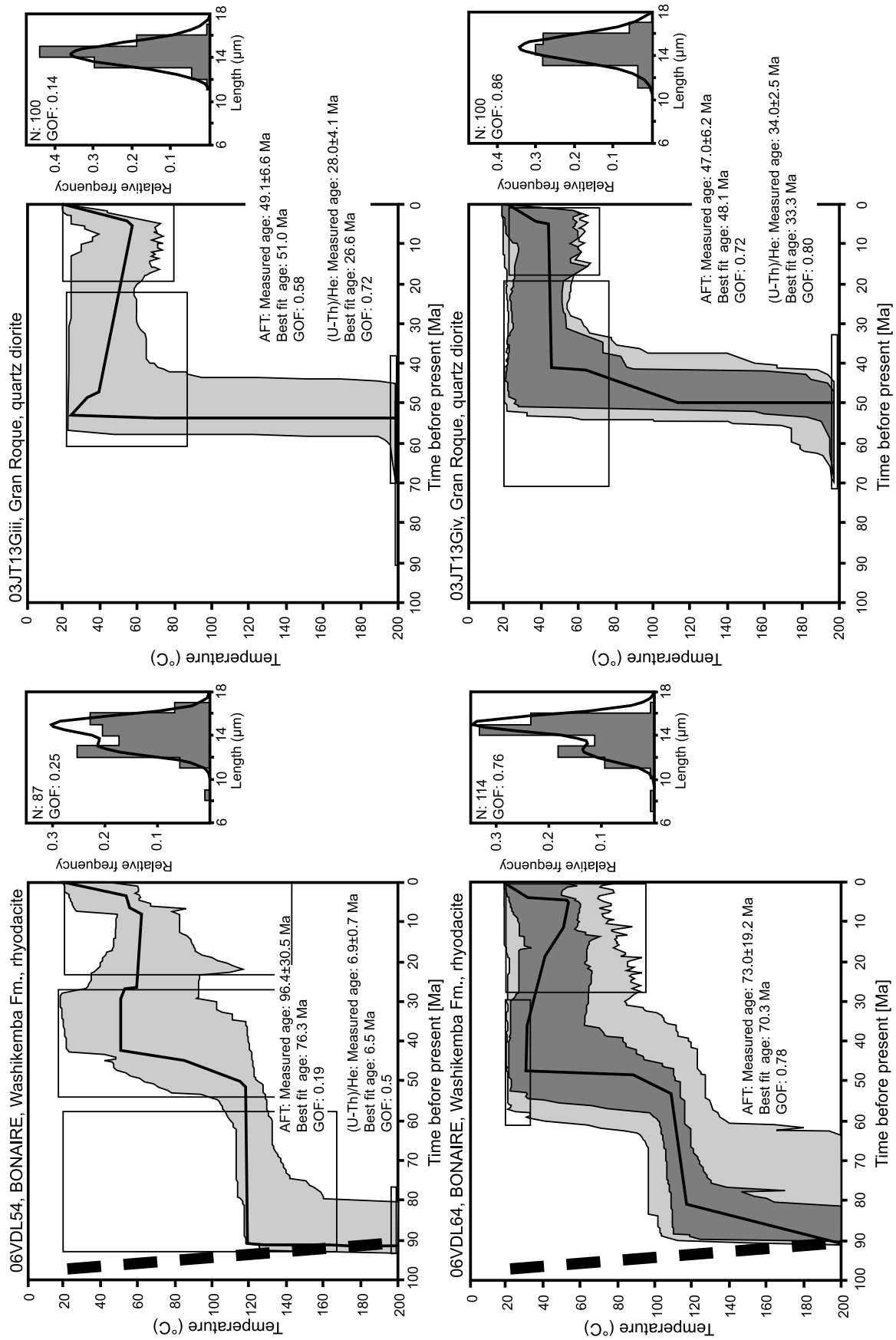

Figure 9. (continued)

al., 1999; *Wright and Wyld*, 2004]. Intrusive magmatism forming the Aruba Batholith commenced at 89.76 ± 0.85 Ma (this study) [see also *Wright and Wyld*, 2004], ≤3 Myr after the Aruba Lava Formation stopped erupting. Felsic intrusions within basalts and gabbros of the Caribbean Plateau, which yield an indistinguishable age to the Aruba Batholith and bear similar subduction related to TTG geochemical signatures, have been found in accreted plateau fragments in Ecuador (Pujilí granite; 85.5 ± 1.4 Ma [*Vallejo et al.*, 2006, 2009]; Figure 1) and Colombia (Buga granite; 90.6 ± 1.4 Ma [*Villagómez et al.*, 2008]), suggesting that the mechanism responsible for tonalite formation may have been widespread along the leading edge of the Caribbean Plate.

[43] Any model for the evolution of the leading margin of the Caribbean Plate must account for a polarity flip in subduction that terminated east dipping subduction and initiated a west dipping subduction zone. The lack of accurate, radiometric data from Cretaceous arc rocks at the present-day margins of the Caribbean Plate precludes an accurate determination of the timing of subduction polarity flip, although previous suggestions cluster at either ~90 Ma [e.g., *Burke*, 1988; *Kerr et al.*, 2003; *Thompson et al.*, 2004], or 120–110 Ma [e.g., *Pindell et al.*, 2005]. Models which support a polarity flip at ~90 Ma assume that an east dipping subduction zone was choked by the buoyant plateau [*Burke*, 1988], forcing the onset of west dipping subduction, resulting in island arc volcanism through the oceanic plateau (e.g., the Aruba Batholith). These models are based on the premise that primitive mantle normalized, negative niobium anomalies have been used to propose an island arc origin for the Aruba tonalites [e.g., *White et al.*, 1999]. A potential caveat in that hypothesis is the extremely short time span (<3 Myr) between the eruption of rocks above a mantle plume, inversion of subduction zone polarity and sufficient subduction to emplace subduction related igneous rocks in the upper plate. Alternatively, *White et al.* [1999] show that the Aruba Batholith yields geochemical characteristics typical of tonalite-trondhjemite-granodiorite suites suggesting they could also be derived from partial melting of an amphibole rich, mafic plateau [e.g., *Condie*, 2005; *Willbold et al.*, 2009]. Hornblende rich mafic members include hornblende-rich meladiorites known locally as "hooibergites" (Figure 3) [*Westermann*, 1932] and amphibolitic inliers have been documented in various accreted fragments of the CCOP. *Vallejo et al.* [2009] report a plateau $^{40}Ar/^{39}Ar$ hornblende age of 84.7 ± 2.23 Ma for the Totoras amphibolite that crops out in the Western Cordillera of Ecuador (Figure 1), which represents a retrogression age from peak metamorphic temperatures of 850°C–800°C [*Beaudon et al.*, 2005], and therefore a minimum age of metamorphic hornblende growth. The Aruba Batholith may have also derived from partial melting of both mafic cumulates and amphibolite-grade metamorphosed oceanic plateau rocks, and may not be related to subduction tectonics. Consequently, those models which imply that subduction polarity changed by choking of an east dipping subduction zone by the oceanic plateau appear more feasible because the intrusion of the Aruba Batholith is not constrained by the amount of time required to drastically alter the subduction regime.

[44] Polarity flip at ~90 Ma is consistent with our thermochronological data for Aruba and Bonaire (Figure 9). The prehnite-pumpellyite metamorphic overprint of rhyolites of the Washikemba Formation (Bonaire) may have occurred via burial during the accumulation of volcanic rocks within a west facing arc (hereafter referred to as the proto-Caribbean Great Arc). Subsequent collision of the eastward drifting plateau with the proto-Caribbean Great Arc at 90–89 Ma resulted in partial underthrusting, shearing, metamorphism and syntectonic partial anatexis of the plateau rocks (Figure 10). The Washikemba Formation experienced rock uplift and exhumation after the late Turonian–early Coniacian, giving rise to the high cooling rates identified during 90–80 Ma (Figure 9). Rock uplift may have been accommodated by thrusts, which rotated the Washikemba Formation, giving rise to a 30°–60° tilt prior to the deposition of the Campanian-Maastrichtian Rincon Formation. Anatexis of amphibole rich mafic rocks within the plateau resulted in the tonalite dominated lithologies of the Aruba Batholith during 89–87 Ma, with tonalite-trondhjemite-granodiorite signatures [*White et al.*, 1999]. Continued convergence between the North American and Farallòn Plates subsequently gave rise to a west dipping subduction zone that persists today, forming the Lesser Antilles Arc (Figure 1).

[45] West dipping subduction commencing in the Albian [*Pindell et al.*, 2006] implies that either the mantle plume (1) erupted to the west of the subduction system, possibly forcing the slab to dip with a steeper angle, or (2) erupted through a slab window caused by the subduction of the proto-Caribbean spreading ridge, permitting the Atlantic spreading cell to rise into thinned oceanic crust and melt by decompression during 88–92 Ma, giving rise to a sequence of hot spot related rocks. These hypotheses preclude tectonic collision between the Washikemba Formation and the oceanic plateau rocks and hence it is not clear how they account for rapid cooling and tilting on Bonaire during 90–80 Ma. Eruption of the mantle plume to the west of the subducting slab implies that MORB would separate the Washikemba Formation from the oceanic plateau. Furthermore, the lack of collision-induced tectonic burial of the oceanic plateau may preclude partial anatexis and the formation of sufficient partial melts to build the Aruba Batholith. Consequently, the Aruba Batholith would be related to subduction, requiring significant flattening of the subducted slab, depending on the amount of MORB that was originally entrained between the Washikemba Formation and the oceanic plateau. Rapid fluctuations in slab dip have been postulated by *Kay et al.* [2006] to account for the lateral extent of Miocene continental arc rocks in central Chile, and may account for rock uplift and exhumation of the Washikemba Formation during flattening between 90 and 80 Ma. Alternatively, upwelling mantle material through a slab window may drive rock uplift in the upper plate, leading to exhumation and cooling of the Washikemba Formation. However, *Hastie and Kerr* [2010] recently utilized physical and geochemical constraints to conclude that the Caribbean oceanic plateau lavas are derived from decompression melting of a hot upwelling mantle plume, and that the slab window model is improbable.

[46] The thermochronological data cannot be used to prove either a collision event at 90 Ma, or polarity flip

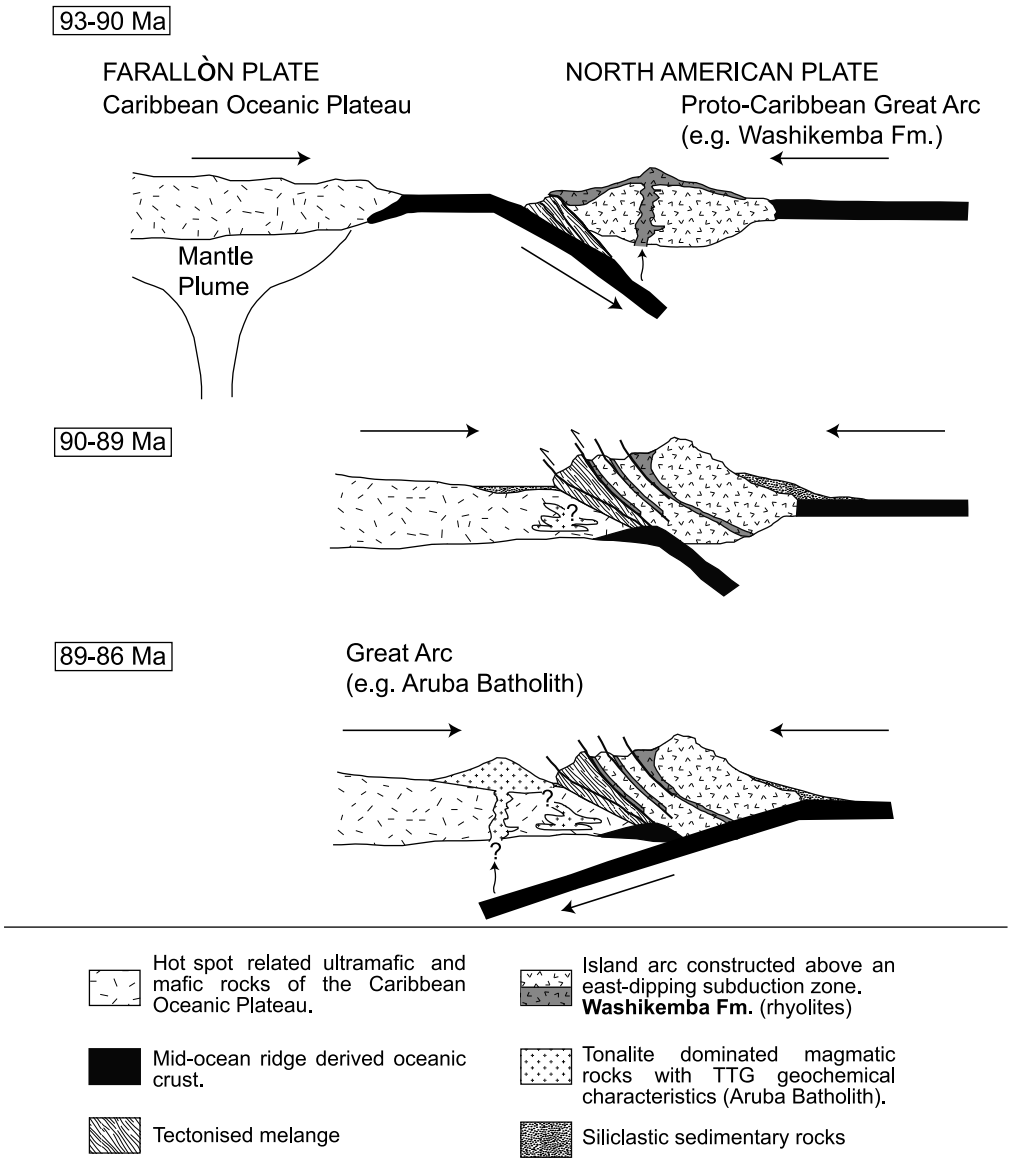

Figure 10. Schematic illustration of the evolution of rocks of the Bonaire Block during subduction polarity flip at 90 Ma. From 93 to 90 Ma: (1) growth of the proto-Caribbean Great Arc above an east dipping subduction zone, resulting in burial metamorphism of the current surface of the Washikemba Formation to prehnite-pumpellyite facies and (2) eruption of rocks above a mantle plume giving rise to the laterally extensive CCOP. From 90 to 89 Ma: (1) collision of the CCOP and proto-Caribbean Great Arc, resulting in deformation, amphibolite-grade regional metamorphism, and localized anatexis of hydrated mafic rocks of the oceanic plateau and (2) thrusting, rotation, rock uplift, and exhumation of the Washikemba Formation. From 89 to 86 Ma: sufficient accumulation of partial melts of the CCOP to generate tonalite-trondhjemite-granodiorite (TTG) intrusions along the margin of the CCOP (e.g., Aruba Batholith and the Buga and Pujilí granites of the northern Andes; Figure 1). These rocks may or may not be related to west dipping subduction, depending on the amount of time required to achieve polarity flip and sufficient subduction.

during the Albian. However, a collision event at ~90–89 Ma is supported by (1) tilting of the Washikemba Formation to a steep angle prior to the Campanian-Maastrichtian, combined with >3 km of exhumation during 90–80 Ma, and (2) syntectonic anatexis of the oceanic plateau (Figure 10). Consequently, we favor a subduction polarity flip event commencing at ~90 Ma, which is evident along at least 1500 km of strike of the southern margin of the accreted plateau, giving rise to the Buga Batholith and Pujilí Granite (Figure 1).

[47] Our new radiometric data agree with previous interpretations suggesting that the metamafic basement of Gran

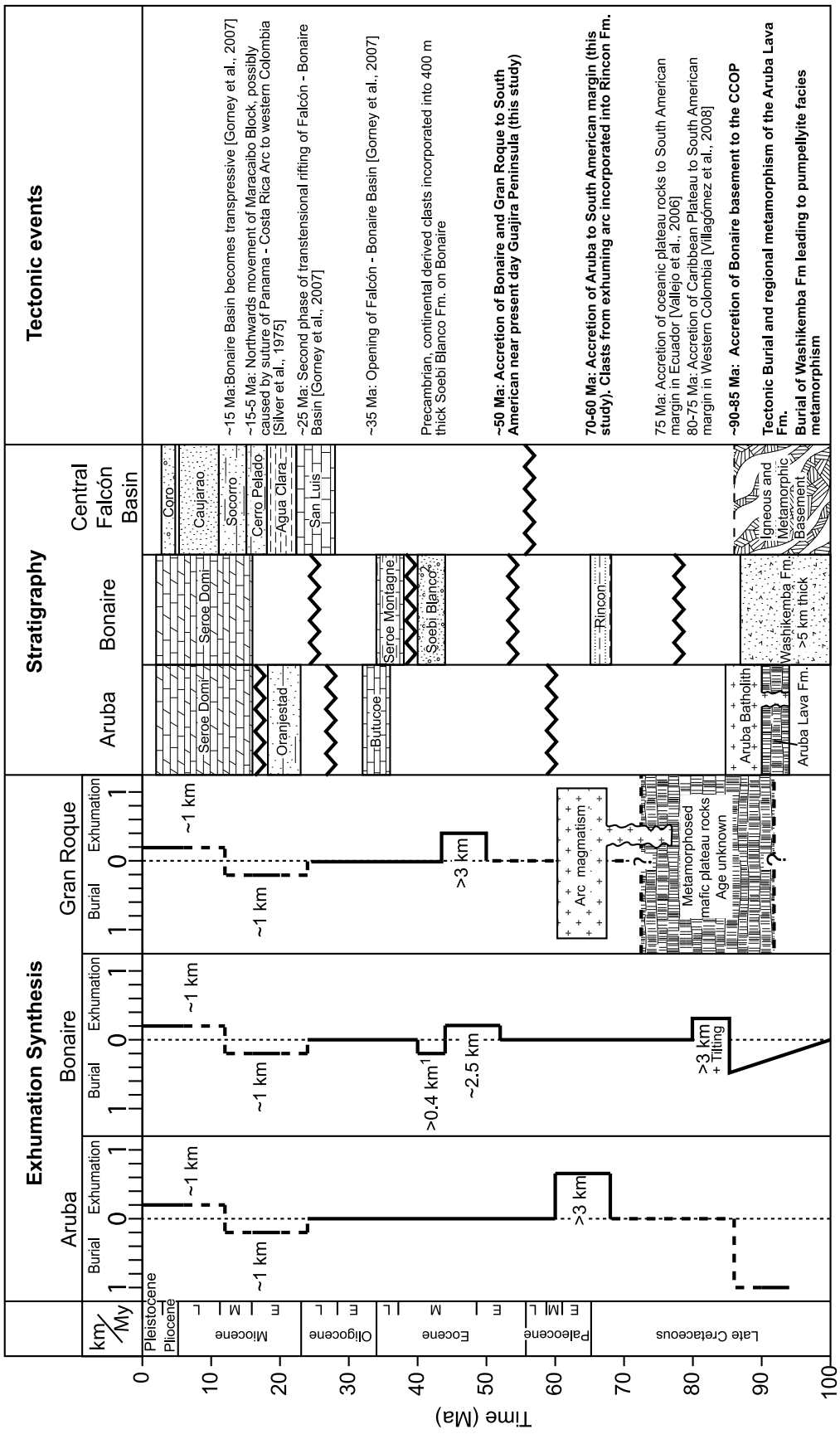

Figure 11. Synthesis of burial and exhumation results, derived from the best fit thermochronological data, assuming a geothermal gradient of 30°C/km. Dashed lines indicate poorly resolved time constraints. Stratigraphic columns are shown for Aruba [*Beets et al.*, 1996], Bonaire [*Beets et al.*, 1977; *Pijpers*, 1933], and the central Falcón Basin [*Macellari*, 1995], and a summary of regional tectonic events is shown, with bold text indicating major events for the studied islands. Here 1, burial amount inferred from strata thickness that unconformably overlies sample 06VDL64; 2, stratigraphic age inferred to be postexhumation. The Soebi Blanco Formation unconformably overlies modeled sample 06VDL64.

Roque was intruded by an island arc sequence at ~65 Ma. Given that the age of onset of subduction beneath the CCOP is probably older than ~89 Ma, the age of the Gran Roque intrusive sequences suggests they may have formed during the eastward migration of the Caribbean Plate. Consequently, they may represent an accreted fragment of the Aves Ridge, which is considered to have been an early component of the present-day Lesser Antilles, prior to the opening of the Grenada Basin [*Aitken et al.*, 2010] (Figure 1). However, the age and nature of the exposed amphibolites and lower greenschist facies gabbros exposed on Gran Roque is still unclear, and may either represent either (1) CCOP plateau material or (2) MORB which was trapped between the west dipping subduction zone and the CCOP.

6.2. Collision and Accretion of the Bonaire Block With the South American Plate

[48] The lack of magmatic activity on Aruba at 70–60 Ma suggests that cooling of >100°C during 70–60 Ma was driven by exhumation of >3 km at rates of ~0.6 km/Myr, assuming an average geothermal gradient of 30°C/km. The onset of exhumation slightly postdates the timing of collision of the CCOP with the Ecuadorian paleomargin at 75–73 Ma [*Spikings et al.*, 2000; *Vallejo et al.*, 2006, 2009], and predates the late Eocene opening of the postaccretionary Bonaire and Falcón basins (Figure 2) [*Curet*, 1992; *Gorney et al.*, 2007]. Therefore, we attribute rapid Maastrichtian-Danian exhumation of Aruba to the collision of the CCOP with the South American Plate, at least 500 km to the west of its current location, relative to the South American Plate (Figure 12).

[49] The basement of Bonaire (Washikemba Formation) underwent a second phase of rapid exhumation of ~2.5 km at ~50 Ma, again assuming a geothermal gradient of 30°C/km (Figure 11). Subsequently, fluvial conglomerates of the Soebi Blanco Formation (Figure 5) were deposited across a geographically widespread unconformity. The conglomerate hosts ~1 Ga (zircon U/Pb [*Priem et al.*, 1986b]) old gneissic clasts, indicating that these conglomerates were deposited within the catchment of Precambrian source regions that were located within the South American Plate, and may have formed part of what is now the Guajira Peninsula [*Priem et al.*, 1986b] (Figure 1). We suggest that exhumation of the Washikemba Formation at ~50 Ma occurred in response to its collision and accretion to the South American Plate (Figure 12). Similarly, *Wright and Wyld* [2004] attribute Danian–middle Eocene folding on the neighboring island of Curaçao (Figure 1) to its accretion with the South American Plate.

[50] Rapid cooling (>80°C) of crystalline rocks on Gran Roque occurred at ~50 Ma (Figure 9), ~15 Myr after intrusion of the arc sequence. The timing of cooling is indistinguishable from that of the second phase of rapid cooling on Bonaire. Given the island's clear intraoceanic origin and its current position as an accreted fragment in the Bonaire Block, we propose that Eocene rapid cooling of the basement rocks of Gran Roque was a result of exhumation driven by accretion to the South Caribbean Plate boundary zone (Figure 12).

[51] The basement rocks of Aruba, Bonaire and Gran Roque have distinctly different crystallization ages and tectonic origins, and define discrete terranes within the Bonaire Block. Furthermore, the timing of collision and accretion of these terranes with the South American plate was probably strongly diachronous (Figure 11), and dependent on the location of those terranes along the leading margin of the eastward advancing Caribbean Plate (Figure 12). The Aruba Batholith and its host Aruba Lava Formation represent a fragment of the CCOP that was located within the collision zone between the CCOP and the South American Plate, and was exhumed in response to that event. However, the basements represented by the Washikemba Formation and Gran Roque were located distant to the initial collision event with the South American Plate and were not exhumed by it. In contrast, during the accretion of Aruba, subduction of the proto-Caribbean seaway was still occurring beneath the mafic basement of Gran Roque, generating island arc magmas (Figure 12). The Washikemba Formation and Gran Roque accreted to the South American Plate after significant dextral displacement, and after the Caribbean Plate started converging with the South American Plate at ~50 Ma [e.g., *Ross and Scotese*, 1988; *Pindell and Barrett*, 1990]. The accretion of the basements of Bonaire and Gran Roque appears to have occurred almost simultaneously, which suggests that during these final stages of amalgamation of the Bonaire Block, the Leeward Antilles may have followed an east-west trend prior to accretion (Figure 12). This is supported by paleomagnetic studies suggesting that the islands have experienced ≤90° rotation since their formation [*Stearns et al.*, 1982].

[52] The geological evolution of the Bonaire Block since 50–45 Ma has been dominated by dextral strike slip displacement between the South American and Caribbean plates. Upper Eocene–lower Oligocene transtensional rifting of the Bonaire-Falcón basin buried the Leeward Antilles [*Gorney et al.*, 2007], resulting in reheating to ~40°C–60°C (Figures 2 and 11). Normal faults were inverted in the middle Miocene as the basin became transpressive [*Gorney et al.*, 2007], resulting in cooling of 20°C–40°C on Aruba,

Figure 12. Schematic paleogeographic model for the Late Cretaceous to Eocene accretion of the Bonaire Block to the South American continent, followed by oblique underthrusting of the Caribbean Plate. A, Aruba; B, Bonaire; C, Curaçao; G, Guajira Peninsula; GR, Gran Roque; PCF, Pujilí-Cauca Fault. The South American Plate (light gray), CCOP plus juxtaposed proto-Caribbean Great Arc (intermediate gray), and accreted Caribbean terranes (dark gray) are shown. The suture between the proto-Caribbean Great Arc and CCOP is drawn just after collision at 89–86 Ma, and the present-day position of the Sierra Nevada de Santa Marta is given for reference. The dashed line within the Caribbean Oceanic Plateau represents the paleoposition of the nonaccreted Caribbean Plateau which is currently exposed [*Kennan and Pindell*, 2009].

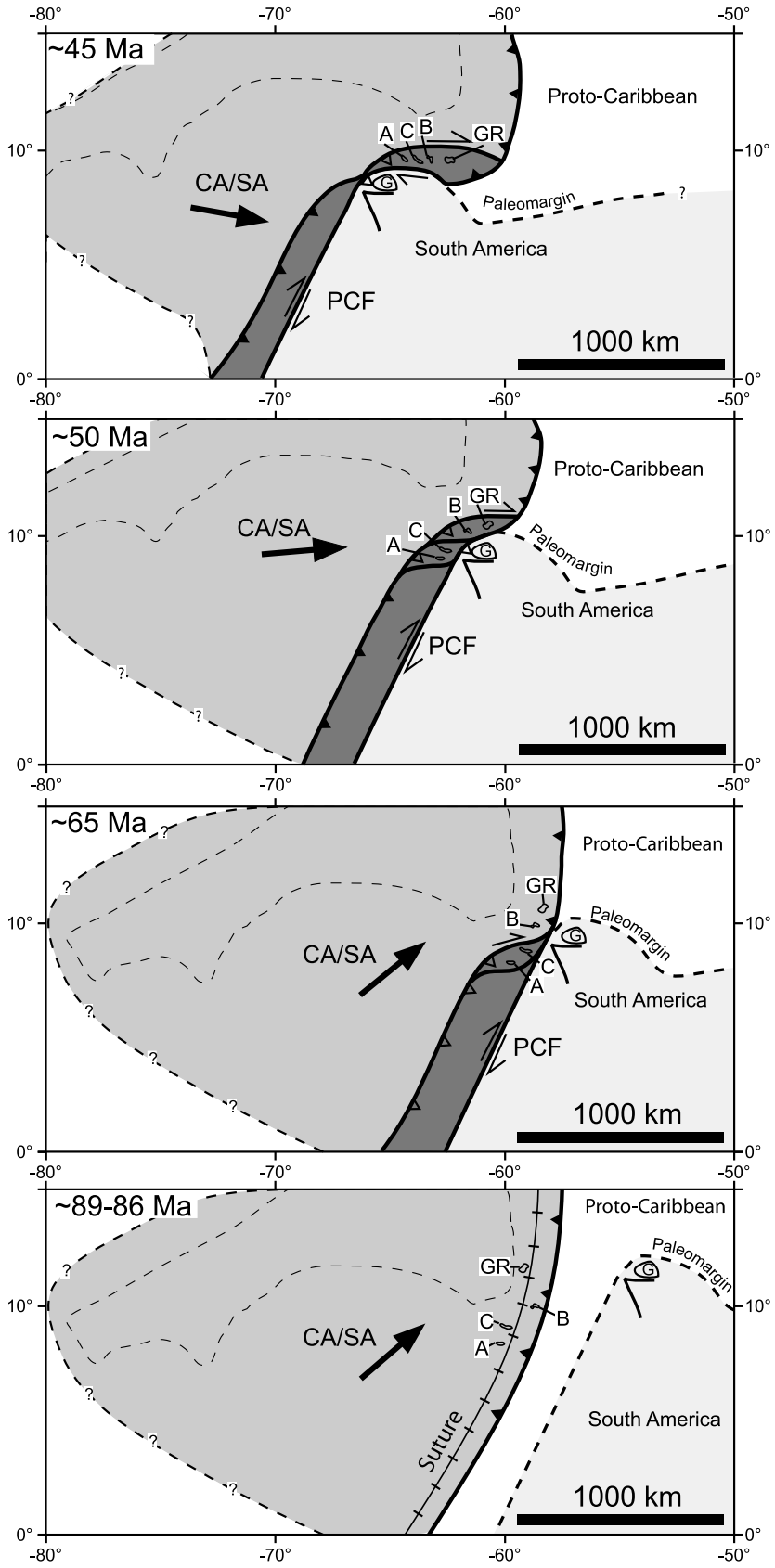
~45 Ma
Proto-Caribbean
A C B GR
CA/SA
Paleomargin
South America
PCF
1000 km
~50 Ma
Proto-Caribbean
B GR
C
A
CA/SA
Paleomargin
South America
PCF
1000 km
~65 Ma
Proto-Caribbean
GR
B
C
A
CA/SA
Paleomargin
South America
PCF
1000 km
~89-86 Ma
Proto-Caribbean
GR
C
A
B
CA/SA
Paleomargin
South America
Suture
1000 km
-80°
-70°
-60°
-50°
10°
0°

Figure 12

Bonaire and Gran Roque until the present day, equating to ~1 km of exhumation since the middle to late Miocene, assuming a geothermal gradient of 30°C/km.

7. Conclusions

[53] We have collected a detailed geochronological and thermochronological data set for several of the Leeward Antilles islands. Combining these new data with field relationships and previous work allows us to place the following constraints on the timing of tectonic events in the South Caribbean Plate Boundary Zone.

[54] 1. The ~90–87 Ma, dominantly tonalitic Aruba Batholith intruded into the Turonian Aruba Lava Formation within 3 Ma of the latter's eruption, subaerial exposure and regional metamorphism. This very short time span implies that the Aruba Batholith may result from rapid subduction polarity reversal at ~85 Ma as suggested by *White et al.* [1999]. Alternatively, the Aruba Batholith may have formed via anatexis of hydrated CCOP basalt and amphibolite during collision of the CCOP with the east dipping proto-Caribbean Great Arc.

[55] 2. The basement of Bonaire (Washikemba Formation) is older than the CCOP and therefore may be a fragment of the east dipping proto-Caribbean Great Arc [*Thompson et al.*, 2004]. The currently exposed surface underwent prehnite-pumpellyite facies metamorphism, retrogression and tilted by 30°–60° before ~80 Ma, which accompanied >3 km of exhumation at rates of ~0.4 km/Myr. Metamorphism was probably driven by burial beneath a volcanic and volcanoclastic pile, whereas exhumation occurred via the erosion of rocks that were uplifted during collision between the Washikemba Formation and the CCOP.

[56] 3. Aruba collided with the South American Plate margin at 70–60 Ma, resulting in >3 km of exhumation. Detritus from the exhuming rocks may have been deposited as pebbles in the Campanian-Maastrichtian Rincon Formation, which is currently preserved on Bonaire.

[57] 4. The basement of Gran Roque consists of metamorphosed MORB or oceanic plateau material that is pre-Tertiary. It was intruded by an island arc sequence at ~65 Ma and hence was structurally separated from the accreting basement of Aruba.

[58] 5. Bonaire collided with the South American Plate margin at ~50 Ma, resulting in ~2.5 km of exhumation. The erosional surface was unconformably overlain by the Paleogene clastic Soebi Blanco Formation, which was at least partly derived from source terranes within the South American Plate.

[59] 6. Gran Roque collided with the South American Plate simultaneously or shortly after Bonaire, at ~50 Ma.

[60] 7. Sequential and diachronous collision of terranes that comprise Aruba, Bonaire and Gran Roque at 70–60 and ~50 Ma resulted in the amalgamation of the Bonaire Block at ~50 Ma. The Bonaire Block has subsequently been entrained within the south Caribbean Plate margin and has been deformed by dextral displacement between the Caribbean and South American plates.

[61] 8. Upper Eocene–lower Oligocene, transtensional rifting in the Bonaire Block opened the Falcón-Bonaire basin, causing the crystalline basement sequences of Aruba, Bonaire and Gran Roque to subside by ~1 km.

[62] 9. Middle to late Miocene transpression drove inversion of the Falcón-Bonaire basin, resulting in rock and surface uplift within the fault blocks that host the Leeward Antilles islands. This was accompanied by ~1 km of exhumation and may predate or be coeval with north directed tectonic escape of the Maracaibo Block from a compressed zone, which may have ultimately been responsible for the dramatic elevation (5.7 km) and relief that is currently exposed in the Sierra Nevada de Santa Marta, northern Colombia (Figure 1). Compressive stresses during this period may have been driven by the collision of the Panama–Costa Rica arc with South America [*Silver et al.*, 1975].

Appendix A

[63] Ground and polished apatite grain mounts for fission track analysis were packed in intimate contact with Brazil Ruby muscovite external detectors following the procedure described by *Gleadow* [1981], and irradiated in the Oregon State University TRIGA reactor. Induced fission tracks were revealed in the mica by etching with 40% HF at ~20°C for 45 min. When sufficient apatite was available, additional grains were mounted in epoxy, polished, irradiated with ^{252}Cf fission fragments [*Donelick and Miller*, 1991] and etched using the same conditions described above to increase the number of measurable horizontal confined fission tracks (TINTs). Spontaneous and induced tracks were counted, and track lengths were measured at 1000x magnification with a dry objective, using a Zeiss Axio Imager microscope equipped with an Autoscan stage. Only inclusion-free grains ground and polished parallel to the crystallographic C axis were counted. Maximum etch pit diameters were measured from each analyzed grain from Aruba and Bonaire to assess the influence of varying annealing kinetics [*Carlson et al.*, 1999]. For samples from Gran Roque, these parameters were assessed using chlorine content [*Carlson et al.*, 1999] determined with a JEOL JXA-5A electron microprobe running at an accelerating voltage of 15 kV, defocused beam size of 15–20 μm and beam current of 29 nA, yielding a standard error of ±15%. Analyses were calibrated using the Durango apatite. Ages were calculated using the Zeta calibration method [*Hurford and Green*, 1983] using the Trackkey program [*Dunkl*, 2002].

[64] **Acknowledgments.** This study was supported by a grant from the Swiss Academy of Sciences, the Augustin Lombard fund of the Geneva SPHN Society, and the Fonds Marc Birkigt. Assistance in field work and logistics was provided by STINAPA Bonaire and Fundacion Parke Arikok, Aruba. The authors are grateful to John Tarney for collecting rock samples on Gran Roque and to Jim Wright for useful discussions on the regional geology and geochronology of the Leeward Antilles. Simon Mitchell and Jim Wright are thanked for their detailed and constructive reviews which helped to dramatically improve this manuscript. Use of the Nordsim was supported by the European Community's program "Structuring the European Research Area" under SYNTHESYS at the Swedish Museum of Natural History, project SE-TAF 663. This is Nordsim publication 261. The Nordsim facility is financed and operated under an agreement between the research councils of Denmark, Norway, and Sweden; the Geological Survey of Finland; and the Swedish Museum of Natural History. Apatites from Aruba and Bonaire were kindly irradiated with ^{252}Cf fission fragments by Ray and Margaret Donelick, Apatite to Zircon, Inc.

References

Aguerrevere, S., and V. M. López (1938), Geologia de la Isla de Gran Roque y sus depósitos de fosfato, *Bol. Geol. Min.*, *2*, 155–181.

Aitken, T., P. Mann, A. Escalona, and G. L. Christeson (2010), Evolution of the Grenada and Tobago basins and implications for arc migration, *Mar. Pet. Geol.*, doi:10.1016/j.marpetgeo.2009.10.003, in press.

Amante, C., and B. Eakins (2008), ETOPO1 1 arc-minute global relief model: Procedures, data sources and analysis, Natl. Geophys. Data Cent., NESDIS, NOAA, U.S. Dep. of Commer., Boulder, Colo.

Audemard, F. A. (1998), Evolution geodynamique de la façade nord Sud-americane: Nouveaux apports de l'histoire géologique du bassin de Falcón, Vénézuela, *Bol. Geol. Publ. Esp.*, *5*, 269–272.

Audemard, F. A., G. Romero, H. Rendon, and V. Cano (2005), Quaternary fault kinematics and stress tensors along the southern Caribbean from fault-slip data and focal mechanism solutions, *Earth Sci. Rev.*, *69*(3–4), 181–233, doi:10.1016/j.earscirev.2004.08.001.

Audemard, F. E., and F. A. Audemard (2002), Structure of the Mérida Andes, Venezuela: Relations with the South America–Caribbean geodynamic interaction, *Tectonophysics*, *345*(1–4), 299–327, doi:10.1016/S0040-1951(01)00218-9.

Baumgartner, P. O., A. Bandini, and P. Denyer (2004), Jurassic–Lower Cretaceous radiolarites in Central America and the Caribbean-remnants of Pacific ocean floor, paper presented at 2nd Swiss Geoscience Meeting, GEOforumCH, Lausanne, Switzerland.

Beardsley, A. G. (2007), Oblique collision and accretion of the Netherlands Leeward Antilles Island Arc: A structural analysis of the Caribbean–South American Plate boundary zone, Ph.D. thesis, Rice Univ., Houston, Tex.

Beaudon, E., J.-E. Martelat, A. Amórtegui, H. Lapierre, and E. Jaillard (2005), Métabasites de la cordillère occidentale d'Équateur, témoins du soubassement océanique des Andes d'Équateur, *C. R. Geosci.*, *337*(6), 625–634, doi:10.1016/j.crte.2005.01.002.

Beets, D. J., H. MacGillavry, and G. Klaver (1977), Geology of the Cretaceous and early Tertiary of Bonaire, *GUA Pap. Geol.*, *1*(10), 18–28.

Beets, D. J., W. V. Maresch, G. T. Klaver, A. Mottana, R. Bocchio, F. F. Beunk, and H. P. Monen (1984), Magmatic rock series and high-pressure metamorphism as constraints on the tectonic history of the southern Caribbean, in *The Caribbean–South American Plate Boundary and Regional Tectonics*, edited by W. E. Bonini, R. B. Hargraves, and R. Shagam, *Mem. Geol. Soc. Am.*, *162*, 95–130.

Beets, D. J., R. Metten, and B. Hoogendoorn (1996), Geological map of Aruba, scale 1:50000, Nat. Stud. voor het Caraïbisch Gebied Rijks Geol. Dienst, Amsterdam.

Bezada, M. J., M. Schmitz, M. I. Jácome, J. Rodríguez, F. Audemard, and C. Izarra (2008), Crustal structure in the Falcón Basin area, northwestern Venezuela, from seismic and gravimetric evidence, *J. Geodyn.*, *45*(4–5), 191–200, doi:10.1016/j.jog.2007.11.002.

Burke, K. (1988), Tectonic evolution of the Caribbean, *Annu. Rev. Earth Planet. Sci.*, *16*(1), 201–230, doi:10.1146/annurev.ea.16.050188.001221.

Carlson, W. D., R. A. Donelick, and R. A. Ketcham (1999), Variability of apatite fission-track annealing kinetics: I. Experimental results, *Am. Mineral.*, *84*(9), 1213–1223.

Condie, K. C. (2005), TTGs and adakites: Are they both slab melts?, *Lithos*, *80*(1–4), 33–44, doi:10.1016/j.lithos.2003.11.001.

Curet, E. A. (1992), Stratigraphy and evolution of the Tertiary Aruba Basin, *J. Pet. Geol.*, *15*(2), 283–304, doi:10.1111/j.1747-5457.1992.tb00873.x.

DeMets, C., P. E. Jansma, G. S. Mattioli, T. H. Dixon, F. Farina, R. Bilham, E. Calais, and P. Mann (2000), GPS geodetic constraints on Caribbean–North America Plate motion, *Geophys. Res. Lett.*, *27*(3), 437–440, doi:10.1029/1999GL005436.

Dewey, J. F., and J. L. Pindell (1985), Neogene block tectonics of eastern Turkey and northern South America: Continental applications of the finite difference method, *Tectonics*, *4*(1), 71–83, doi:10.1029/TC004i001p00071.

Donelick, R. A. (1991), Crystallographic orientation dependence of mean etchable fission track length in apatite: An empirical model and experimental observations, *Am. Mineral.*, *76*(1–2), 83–91.

Donelick, R. A., and D. S. Miller (1991), Enhanced TINT fission track densities in low spontaneous track density apatites using ^{252}Cf-derived fission fragment tracks: A model and experimental observations, *Nucl. Tracks Radiat. Meas.*, *18*(3), 301–307, doi:10.1016/1359-0189(91)90022-A.

Donelick, R. A., R. A. Ketcham, and W. D. Carlson (1999), Variability of apatite fission-track annealing kinetics: II. Crystallographic orientation effects, *Am. Mineral.*, *84*(9), 1224–1234.

Dunkl, I. (2002), TRACKKEY: A Windows program for calculation and graphical presentation of fission track data, *Comput. Geosci.*, *28*(1), 3–12, doi:10.1016/S0098-3004(01)00024-3.

Edgar, N. T., J. I. Ewing, and J. Hennion (1971), Seismic refraction and reflection in Caribbean Sea, *AAPG Bull.*, *55*, 833–870.

Farley, K. A., and D. F. Stockli (2002), (U-Th)/He dating of phosphates: Apatite, monazite, and xenotime, *Rev. Mineral. Geochem.*, *48*(1), 559–577, doi:10.2138/rmg.2002.48.15.

Fitzgerald, P. G., S. L. Baldwin, L. E. Webb, and P. B. O'Sullivan (2006), Interpretation of (U-Th)/He single grain ages from slowly cooled crustal terranes: A case study from the Transantarctic Mountains of southern Victoria Land, *Chem. Geol.*, *225*(1–2), 91–120, doi:10.1016/j.chemgeo.2005.09.001.

Flowers, R. M., R. A. Ketcham, D. L. Shuster, and K. A. Farley (2009), Apatite (U-Th)/He thermochronometry using a radiation damage accumulation and annealing model, *Geochim. Cosmochim. Acta*, *73*(8), 2347–2365, doi:10.1016/j.gca.2009.01.015.

Giunta, G., L. Beccaluva, M. Coltorti, F. Siena, and C. Vaccaro (2002), The southern margin of the Caribbean Plate in Venezuela: Tectono-magmatic setting of the ophiolitic units and kinematic evolution, *Lithos*, *63*(1–2), 19–40, doi:10.1016/S0024-4937(02)00120-2.

Gleadow, A. J. W. (1981), Fission-track dating methods: What are the real alternatives?, *Nucl. Tracks*, *5*(1–2), 3–14, doi:10.1016/0191-278X(81)90021-4.

Gorney, D., A. Escalona, P. Mann, M. B. Magnani, and BOLIVAR Study Group (2007), Chronology of Cenozoic tectonic events in western Venezuela and the Leeward Antilles based on integration of offshore seismic reflection data and on-land geology, *AAPG Bull.*, *91*, 653–684, doi:10.1306/11280606002.

Gradstein, F. M., J. G. Ogg, and A. G. Smith (2004), *A Geologic Time Scale 2004*, Cambridge Univ. Press, Cambridge, U. K.

Hastie, A. R., and A. C. Kerr (2010), Mantle plume or slab window?: Physical and geochemical constraints on the origin of the Caribbean oceanic plateau, *Earth Sci. Rev.*, *98*(3–4), 283–293, doi:10.1016/j.earscirev.2009.11.001.

Helmers, H., and D. J. Beets (1977), Geology of the Cretaceous of Aruba, *GUA Pap. Geol.*, *1*(10), 29–35.

Hurford, A. J., and P. F. Green (1983), The zeta age calibration of fission-track dating, *Chem. Geol.*, *41*(4), 285–317, doi:10.1016/S0009-2541(83)80026-6.

James, K. (2006), Arguments for and against the Pacific origin of the Caribbean Plate: Discussion, finding for an inter-American origin, *Geol. Acta*, *4*(1–2), 279–302.

Kauffman, E. G. (1978), Middle Cretaceous bivalve zones and stage implications in the Antillean Subprovince, Caribbean Province, *Ann. Mus. Hist. Nat. Nice*, *4*(17), 1–6.

Kay, S. M., W. M. Burns, P. Copeland, and O. Mancilla (2006), Upper Cretaceous to Holocene magmatism and evidence for transient Miocene shallowing of the Andean subduction zone under the northern Neuquén Basin, *Spec. Pap. Geol. Soc. Am.*, *407*, 19–60.

Kellogg, J. (1984), Cenozoic tectonic history of the Sierra de Perijá, Venezuela-Colombia, and adjacent basins, *Mem. Geol. Soc. Am.*, *162*, 239–261.

Kennan, L., and J. L. Pindell (2009), Dextral shear, terrane accretion and basin formation in the Northern Andes: Best explained by interaction with a Pacific-derived Caribbean Plate, in *The Origin and Evolution of the Caribbean Plate*, edited by K. H. James, M. A. Lorente, and J. L. Pindell, *Geol. Soc. Spec. Publ.*, *328*, 487–531.

Kerr, A. C., J. Tarney, G. F. Marriner, A. Nivia, G. T. Klaver, and A. D. Saunders (1996), The geochemistry and tectonic setting of Late Cretaceous Caribbean and Colombian volcanism, *J. South Am. Earth Sci.*, *9*(1–2), 111–120, doi:10.1016/0895-9811(96)00031-4.

Kerr, A. C., R. V. White, P. M. E. Thompson, J. Tarney, and A. S. Saunders (2003), No oceanic plateau; no Caribbean Plate? The seminal role of an oceanic plateau in Caribbean Plate evolution, *AAPG Mem.*, *79*, 126–168.

Ketcham, R. A. (2005), Forward and inverse modeling of low-temperature thermochronometry data, *Rev. Mineral. Geochem.*, *58*(1), 275–314, doi:10.2138/rmg.2005.58.11.

Ketcham, R. A., R. A. Donelick, and W. D. Carlson (1999), Variability of apatite fission-track annealing kinetics: III. Extrapolation to geological time scales, *Am. Mineral.*, *84*(9), 1235–1255.

Klaver, G. (1976), The Washikemba Formation, Bonaire, M.Sc. thesis, Utrecht Univ., Utrecht, Netherlands.

Kohn, B. P., R. Shagam, P. O. Banks, and L. A. Burkley (1984), Mesozoic-Pleistocene fission-track ages on rocks of the Venezuelan Andes and their tectonic implications, *Mem. Geol. Soc. Am.*, *162*, 365–384.

Koppers, A. A. P. (2002), ArArCALC—Software for ^{40}Ar/^{39}Ar age calculations, *Comput. Geosci.*, *28*(5), 605–619, doi:10.1016/S0098-3004(01)00095-4.

Ludwig, K. R. (2003), *User's Manual for Isoplot 3.00: A Geochronological Toolkit for Microsoft Excel*, *Berkeley Geochronol. Cent. Spec. Publ.*, *4*, 70 pp.

Luzieux, L. D. A., F. Heller, R. Spikings, C. F. Vallejo, and W. Winkler (2006), Origin and Cretaceous tectonic history of the coastal Ecuadorian forearc between 1°N and 3°S: Paleomagnetic, radiometric and fossil evidence, *Earth Planet. Sci. Lett.*, *249*(3–4), 400–414, doi:10.1016/j.epsl.2006.07.008.

MacDonald, W. D. (1968), Communication, *Status Geol. Res. Caribbean*, *14*, 40–41.

Macellari, C. E. (1995), Cenozoic sedimentation and tectonics of the southwestern Caribbean pull-apart basin, Venezuela and Colombia, in *Petroleum Basins of South America*, edited by A. J. Tankard, R. Suárez Soruco, and H. J. Welsink, *AAPG Mem.*, *62*, 757–780.

Mann, P., and K. Burke (1984), Neotectonics of the Caribbean, *Rev. Geophys.*, *22*, 309–362.

Marschik, R., R. A. Spikings, and I. Kuscu (2008), Geochronology and stable isotope signature of alteration related to hydrothermal magnetite ores in central Anatolia, Turkey, *Miner. Deposita*, *43*(1), 111–124, doi:10.1007/s00126-007-0160-4.

Meschede, M., and W. Frisch (1998), A plate-tectonic model for the Mesozoic and Early Cenozoic history of the Caribbean plate, *Tectonophysics*, *296*(3–4), 269–291, doi:10.1016/S0040-1951(98)00157-7.

Mitchell, S. F., and R. Ramsook (2009), Rudist bivalve assemblages from the Back Rio Grande Formation

(Cretaceous: Campanian) of Jamaica and their stratigraphic significance, *Cretaceous Res.*, *30*, 307–321, doi:10.1016/j.cretres.2008.07.009.

Molina, A. C., U. G. Cordani, and W. D. MacDonald (2006), Tectonic correlations of pre-Mesozoic crust from the northern termination of the Colombian Andes, Caribbean region, *J. South Am. Earth Sci.*, *21*(4), 337–354, doi:10.1016/j.jsames.2006.07.009.

Montgomery, H., E. A. Pessagno Jr., J. F. Lewis, and J. Schellekens (1994), Paleogeography of Jurassic fragments in the Caribbean, *Tectonics*, *13*(3), 725–732, doi:10.1029/94TC00455.

Norabuena, E. O., T. H. Dixon, S. Stein, and C. G. A. Harrison (1999), Decelerating Nazca–South America and Nazca–Pacific plate motions, *Geophys. Res. Lett.*, *26*(22), 3405–3408.

Ostos, M., and V. B. Sisson (2005), Geochemistry and tectonic setting of igneous and metaigneous rocks of northern Venezuela, *Spec. Pap. Geol. Soc. Am.*, *394*, 119–156.

Philpotts, A. R. (1990), *Principles of Igneous and Metamorphic Petrology*, 498 pp., Prentice-Hall, Englewood Cliffs, N. J.

Pijpers, P. J. (1933), *Geology and Paleontology of Bonaire (D. W. I.)*, *Geogr. Geol. Meded. Physiogr. Geol. Reeks*, *8*, 103 pp.

Pindell, J., and S. Barrett (1990), Geological evolution of the Caribbean region: A plate-tectonic perspective, in *The Caribbean Region*, edited by G. Dengo and J. E. Case, pp. 405–432, Geol. Soc. of Am., Boulder, Colo.

Pindell, J., and J. F. Dewey (1982), Permo-Triassic reconstruction of western Pangea and the evolution of the Gulf of Mexico/Caribbean region, *Tectonics*, *1*(2), 179–211, doi:10.1029/TC001i002p00179.

Pindell, J., L. Kennan, W. V. Maresch, K. Stanek, G. Draper, and R. Higgs (2005), Plate-kinematics and crustal dynamics of circum-Caribbean arc-continent interactions: Tectonic controls on basin development in proto-Caribbean margins, *Spec. Pap. Geol. Soc. Am.*, *394*, 7–52.

Pindell, J., L. Kennan, G. Draper, W. V. Maresch, and K. P. Stanek (2006), Foundations of Gulf of Mexico and Caribbean evolution: Eight controversies resolved, *Geol. Acta*, *4*(1–2), 303–341.

Priem, H. N. A. (1979), K-Ar and Rb-Sr dating in the Cretaceous island arc succession of Bonaire, Netherlands Antilles, *Geol. Mijnbouw*, *58*, 367–373.

Priem, H. N. A., N. Boelrijk, R. H. Verschure, E. H. Hebeda, and R. A. Lagaay (1966), Isotopic age of the quartz-diorite batholith on the island of Aruba, Netherlands Antilles, *Geol. Mijnbouw*, *45*, 188–190.

Priem, H. N. A., P. A. M. Andriessen, D. J. Beets, N. Boelrijk, E. A. Verdurmen, and R. H. Verschure (1977), Isotopic dating in the crystalline core of Bonaire, Netherlands Antilles: A progress report, in *8th Caribbean Geological Conference, Curaçao*, edited by H. J. MacGillavry and D. Beets, pp. 192–193, Geol. Mijnbouw, Utrecht, Netherlands.

Priem, H. N. A., D. J. Beets, N. Boelrijk, E. H. Hebeda, E. A. Verdurmen, and R. H. Verschure (1978), Rb-Sr evidence for episodic intrusion of the Late Cretaceous tonalitic batholith of Aruba, Netherlands Antilles, *Geol. Mijnbouw*, *57*, 293–296.

Priem, H. N. A., D. J. Beets, N. Boelrijk, and E. H. Hebeda (1986a), On the age of the Late Cretaceous tonalitic/gabbroic batholith on Aruba, Netherlands Antilles (southern Caribbean borderland), *Geol. Mijnbouw*, *65*, 247–265.

Priem, H. N. A., D. J. Beets, and E. A. Verdurmen (1986b), Precambrian rocks in an early Tertiary conglomerate on Bonaire, Netherlands Antilles (South Caribbean borderland): Evidence for a 300 km eastward displacement relative to the South American mainland, *Geol. Mijnbouw*, *65*, 35–40.

Ross, M. I., and C. R. Scotese (1988), A hierarchical tectonic model of the Gulf of Mexico and Caribbean region, *Tectonophysics*, *155*(1–4), 139–168, doi:10.1016/0040-1951(88)90263-6.

Santamaría, F., and C. Schubert (1974), Geochemistry and geochronology of the southern Caribbean-northern Venezuela Plate boundary, *Geol. Soc. Am. Bull.*, *85*(7), 1085–1098, doi:10.1130/0016-7606(1974)85<1085:GAGOTS>2.0.CO;2.

Shuster, D. L., and K. A. Farley (2009), The influence of artificial radiation damage and thermal annealing on helium diffusion kinetics in apatite, *Geochim. Cosmochim. Acta*, *73*(1), 183–196, doi:10.1016/j.gca.2008.10.013.

Silver, E. A., J. E. Case, and H. J. MacGillavry (1975), Geophysical study of the Venezuelan borderland, *Geol. Soc. Am. Bull.*, *86*(2), 213–226, doi:10.1130/0016-7606(1975)86<213:GSOTVB>2.0.CO;2.

Sinton, C., R. Duncan, M. Storey, J. Lewis, and J. Estrada (1998), An oceanic flood basalt province within the Caribbean Plate, *Earth Planet. Sci. Lett.*, *155*(3–4), 221–235, doi:10.1016/S0012-821X(97)00214-8.

Solé, J., and T. Pi (2005), An empirical calibration for ^{4}He quantification in minerals and rocks by laser fusion and noble gas mass spectrometry using Cerro de Mercado (Durango, Mexico) fluorapatite as a standard, *Anal. Chim. Acta*, *535*(1–2), 325–330, doi:10.1016/j.aca.2004.12.020.

Spikings, R. A., D. Seward, W. Winkler, and G. M. Ruiz (2000), Low-temperature thermochronology of the northern Cordillera Real, Ecuador: Tectonic insights from zircon and apatite fission track analysis, *Tectonics*, *19*(4), 649–668, doi:10.1029/2000TC900010.

Spikings, R. A., W. Winkler, R. A. Hughes, and R. Handler (2005), Thermochronology of allochthonous terranes in Ecuador: Unravelling the accretionary and post-accretionary history of the Northern Andes, *Tectonophysics*, *399*(1–4), 195–220, doi:10.1016/j.tecto.2004.12.023.

Stacey, J. S., and J. D. Kramers (1975), Approximation of terrestrial lead isotope evolution by a two-stage model, *Earth Planet. Sci. Lett.*, *26*(2), 207–221.

Stearns, C., F. J. Mauk, and R. Van der Voo (1982), Late Cretaceous–early Tertiary paleomagnetism of Aruba and Bonaire (Netherlands Leeward Antilles), *J. Geophys. Res.*, *87*, 1127–1141, doi:10.1029/JB087iB02p01127.

Steiger, R. H., and E. Jäger (1977), Subcommission on geochronology: Convention on the use of decay constants in geochronology and cosmochronology, *Earth Planet. Sci. Lett.*, *36*(3), 359–362.

Thompson, P. M. E., P. D. Kempton, R. V. White, A. D. Saunders, A. C. Kerr, J. Tarney, and M. S. Pringle (2004), Elemental, Hf-Nd isotopic and geochronological constraints on an island arc sequence associated with the Cretaceous Caribbean plateau: Bonaire, Dutch Antilles, *Lithos*, *74*(1–2), 91–116, doi:10.1016/j.lithos.2004.01.004.

Vallejo, C., R. A. Spikings, L. Luzieux, W. Winkler, D. Chew, and L. Page (2006), The early interaction between the Caribbean Plateau and the NW South American Plate, *Terra Nova*, *18*(4), 264–269.

Vallejo, C., W. Winkler, R. A. Spikings, L. Luzieux, F. Heller, and F. Bussy (2009), Mode and timing of terrane accretion in the forearc of the Andes in Ecuador, *Mem. Geol. Soc. Am.*, *204*, 197–216.

van der Hilst, R., and P. Mann (1994), Tectonic implications of tomographic images of subducted lithosphere beneath northwestern South America, *Geology*, *22*(5), 451–454, doi:10.1130/0091-7613(1994)022<0451:TIOTIO>2.3.CO;2.

Villagómez, D., R. A. Spikings, D. Seward, T. Magna, and W. Winkler (2008), New thermochronological constraints on the tectonic history of western Colombia, in *11th International Conference on Thermochronometry*, edited by J. I. Garver, pp. 253–255, Union College, Schenectady, N. Y.

Westermann, J. H. (1932), *The Geology of Aruba*, *Geogr. Geol. Meded. Physiogr. Geol. Reeks*, *7*, 129 pp.

White, R. V., J. Tarney, A. C. Kerr, A. D. Saunders, P. D. Kempton, M. S. Pringle, and G. T. Klaver (1999), Modification of an oceanic plateau, Aruba, Dutch Caribbean: Implications for the generation of continental crust, *Lithos*, *46*(1), 43–68, doi:10.1016/S0024-4937(98)00061-9.

Whitehouse, M. J., and B. S. Kamber (2005), Assigning dates to thin gneissic veins in high-grade metamorphic terranes: A cautionary tale from Akilia, southwest Greenland, *J. Petrol.*, *46*(2), 291–318.

Wiedmann, J. (1978), Ammonites from the Curaçao Lava Formation, Curaçao, Caribbean, *Geol. Mijnbouw*, *57*, 361–364.

Willbold, M., E. Hegner, A. Stracke, and A. Rocholl (2009), Continental geochemical signatures in dacites from Iceland and implications for models of early Archaean crust formation, *Earth Planet. Sci. Lett.*, *279*(1–2), 44–52, doi:10.1016/j.epsl.2008.12.029.

Wright, J. E., and S. J. Wyld (2004), Aruba and Curacao: Remnants of a collided Pacific oceanic plateau? Initial geologic results from the BOLIVAR project, *Eos Trans. AGU*, *85*(47), Fall Meet. Suppl., Abstract T33B-1367.

Zeck, H. P., and M. J. Whitehouse (1999), Hercynian, Pan-African, Proterozoic and Archean ion-microprobe zircon ages for a Betic-Rif core complex, Alpine belt, W Mediterranean—Consequences for its P-T-t path, *Contrib. Mineral. Petrol.*, *134*(2–3), 134–149.

D. Chew, Department of Geology, School of Natural Sciences, Trinity College, Dublin 2, Ireland.

M. Cosca, U.S. Geological Survey, Box 25046, MS 963, Denver, CO 80225-0046, USA.

A. C. Kerr, School of Earth and Ocean Sciences, Cardiff University, Park Place, Cardiff CF10 3YE, UK.

A. Kounov, Institute of Geology and Paleontology, University of Basel, Bernoullistr. 32, CH-4056 Basel, Switzerland.

R. A. Spikings, R. van der Lelij, and D. Villagomez, Department of Mineralogy, University of Geneva, Rue des Maraîchers, 13, CH-1205 Geneva, Switzerland. (roelant.vanderlelij@unige.ch)